

Massive open star clusters using the VVV survey[★]

I. Presentation of the data and description of the approach

A.-N. Chené^{1,2}, J. Borissova^{1,3}, J. R. A. Clarke^{1,4}, C. Bonatto⁵, D. J. Majaess⁶, C. Moni Bidin², S. E. Sale^{1,7}, F. Mauro², R. Kurtev¹, G. Baume⁸, C. Feinstein⁸, V. D. Ivanov⁹, D. Geisler², M. Catelan^{3,7}, D. Minniti^{3,7,10,11}, P. Lucas⁴, R. de Grijs¹² and M. S. N. Kumar¹³

¹ Departamento de Física y Astronomía, Universidad de Valparaíso, Av. Gran Bretaña 1111, Playa Ancha, Casilla 5030, Chile
 e-mail: andrenicolas.chene@gmail.com

² Departamento de Astronomía, Universidad de Concepción, Casilla 160-C, Chile

³ The Milky Way Millennium Nucleus, Av. Vicuña Mackenna 4860, 782-0436 Macul, Santiago, Chile

⁴ University of Hertfordshire, Hatfield, AL10 9AB, UK

⁵ Universidade Federal do Rio Grande do Sul, Departamento de Astronomia CP 15051, RS, Porto Alegre, 91501-970, Brazil

⁶ Saint Marys University, Halifax, Nova Scotia, Canada

⁷ Pontificia Universidad Católica de Chile, Facultad de Física, Departamento de Astronomía y Astrofísica, Av. Vicuña Mackenna 4860, 782-0436 Macul, Santiago, Chile

⁸ Facultad de Ciencias Astronómicas y Geofísicas (UNLP), Instituto de Astrofísica de La Plata (CONICET, UNLP), Paseo del Bosque s/n, La Plata, Argentina

⁹ European Southern Observatory, Ave. Alonso de Cordova 3107, Casilla 19, Chile

¹⁰ Vatican Observatory, V00120 Vatican City State, Italy

¹¹ Department of Astrophysical Sciences, Princeton University, Princeton NJ 08544-1001

¹² Kavli Institute for Astronomy and Astrophysics, Peking University, Yi He Yuan Lu 5, Hai Dian District, Beijing 100871, China

¹³ Centro de Astrofísica da Universidade do Porto, Rua das Estrelas, 4150-762 Porto, Portugal

Received February 17, 2012; accepted June 27, 2012

ABSTRACT

Context. The ESO Public Survey “VISTA Variables in the Vía Láctea” (VVV) provides deep multi-epoch infrared observations for an unprecedented 562 sq. degrees of the Galactic bulge, and adjacent regions of the disk.

Aims. The VVV observations will foster the construction of a sample of Galactic star clusters with reliable and homogeneously derived physical parameters (e.g., age, distance, and mass, etc.). In this first paper in a series, the methodology employed to establish cluster parameters for the envisioned database are elaborated upon by analyzing a subsample of 4 known young open clusters: Danks 1, Danks 2, RCW 79, and DBS 132. The analysis offers a first glimpse of the information that can be gleaned for the final cluster database from the VVV observations.

Methods. Wide-field, deep *JHK_s* VVV observations, combined with new infrared spectroscopy, are employed to constrain fundamental parameters for a subset of clusters.

Results. Results inferred from the deep near-infrared photometry which features mitigated uncertainties (e.g. the accuracy of the photometry is better than 0.1 mag for $K_s < 18$ mag), the wide field-of-view of the VVV survey, and numerous high quality low resolution spectra (typically more than 10 per cluster), are used to establish independent cluster parameters which enable existing determinations to be assessed. An anomalous reddening law in the direction toward the Danks’ clusters is found, i.e. $E(J-H)/E(H-K_s) = 2.20 \pm 0.06$, which exceeds published values for the inner Galaxy. The G305 star forming complex, which includes the Danks’ clusters, lies beyond the Sagittarius-Carina spiral arm and occupies the Centaurus arm. Finally, the first deep infrared color-magnitude diagram of RCW 79 is presented which reveal a sizable pre-main sequence population. A list of candidate variable stars in G305 region is reported.

Conclusions. This study demonstrates the strength of the dataset and methodology employed, and constitutes the first step of a broader study which shall include reliable parameters for a sizable fraction of poorly characterize (& newly discovered) clusters.

Key words. Galaxy: open clusters and associations: general – open clusters and associations: individual: Danks 1, Dank 2, DBS 132, RCW 79 – infrared: stars – surveys

1. Introduction

It is commonly accepted that the majority of stars with masses $\geq 0.50 M_\odot$ form in clustered environments (e.g. Lada & Lada 2003, de Wit et al. 2005), rather than individually. Our location

within our own Galaxy gives us a unique perspective from which we can study star clusters in great detail and such studies have important implications for our understanding of the formation of large galaxies in general.

Estimates indicate that the Milky Way (MW) presently hosts 23000–37000 or more star clusters (Portegies Zwart et al. 2010). However, only 2135 open clusters have been identified (according to the 26 Jan 2012 version of Dias et al. 2002), which constitute a sample affected by several well known selection effects

[★] Based on observations made with NTT telescope at the La Silla Observatory, ESO, under programme ID 087.D-0490A, and with the Clay telescope at the Las Campanas Observatory under programme CN2011A-086. Also based on data from the VVV survey observed under program ID 172.B-2002.

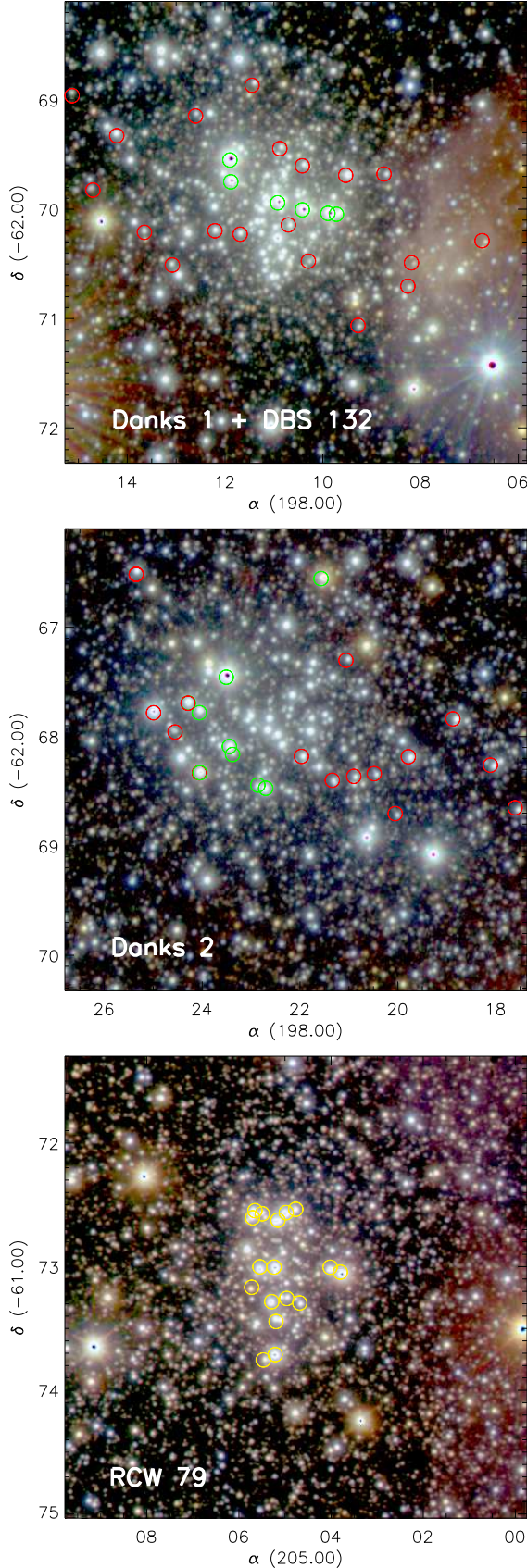


Fig. 1. JHK_s true color images of the three clusters. Stars marked by circles were observed using near infrared spectrographs. In green are the stars observed using SofI at NTT and in red are the stars observed with MMIRS at the Clay telescope. The stars marked with a yellow circle in RCW 79 were already observed by Martins et al. (2010) and, hence, were not re-observed by us.

(same as for globular clusters; Ivanov et al. 2005). Less than half of these clusters have actually been studied, and this subset suffers from further selection biases. Extending this current sample towards the Milky Way's highly obscured and central parts would provide unique insight into the formation, evolution, and dissipation of open clusters in the Galactic environment. To achieve this goal, we are using the unprecedented deep infrared data from the VISTA Variables in the Vía Láctea (VVV) survey (Minniti et al. 2010, Saito et al. 2012), one of the six ESO Public Surveys selected to operate with the new 4-meter Visible and Infrared Survey Telescope for Astronomy (VISTA). We are in the process of building a large sample of star clusters (including many discovered by our group; Borissova et al. 2011, Bonatto et al. in prep), that are practically invisible in the optical bands. The strength of this sample will be the homogeneously derived (i.e. all observed with the same instrument and set-up, and analyzed with the same set of stellar models and isochrones) physical clusters' parameters, including angular sizes, radial velocities (RVs), reddening, distances, masses, and ages. Moreover, as pointed out by Majaess et al. (2012), VVV photometry allows the determination of these parameters with unprecedented accuracy for highly obscured clusters.

As a first step, we are focusing our efforts on the young open clusters in their first few Myrs, during which stars are still forming and the cluster contains a significant amount of gas (i.e. in the Phase I, according to recent classification of Portegies Zwart et al. 2010). The evolution of the cluster during this phase is a complex mixture of gas dynamics, stellar dynamics, stellar evolution, and radiative transfer, and it is currently not completely understood (Elmegreen 2007, Price & Bate 2009). Thus many basic (and critical) cluster properties, such as the duration and efficiency of the star-formation process, the cluster survival probability and the stellar mass function at the beginning of the next phase are uncertain.

In this paper, we present a first sub-sample of 3 known young open clusters using both VVV color-magnitude diagrams (CMDs) and low resolution near-infrared spectroscopy of the brightest stellar members. Those clusters are RCW 79, already studied by Martins et al. (2010), and Danks 1 and Danks 2, presented in Davies et al. (2012). We aim to present a first glimpse into the data quality, and to describe our approach. We also describe our approach for determining the physical parameters of clusters observed with VVV, using previous works as references. Since DBS 132 is positioned close to Danks 1 and Danks 2, we could also get its CMDs and derived some preliminary cluster parameters.

We present the data in Section 2, report our analysis, describe our method and evaluate the accuracy of our work in Section 3, describe the stellar variability detected in the clusters and their surroundings in Section 4, and compare our results with previous studies and discuss briefly the characteristics of the star-forming regions in which the clusters are situated in Section 5 before we summarize this work in Section 6.

2. Observations

2.1. Photometry

2.1.1. VVV data and photometry extraction

We downloaded from the VISTA Science Archive (VSA) website¹ the stacked images of the individual 2048×2048 pixel exposures containing the three clusters presented in this paper.

¹ <http://horus.roe.ac.uk/vsa/>

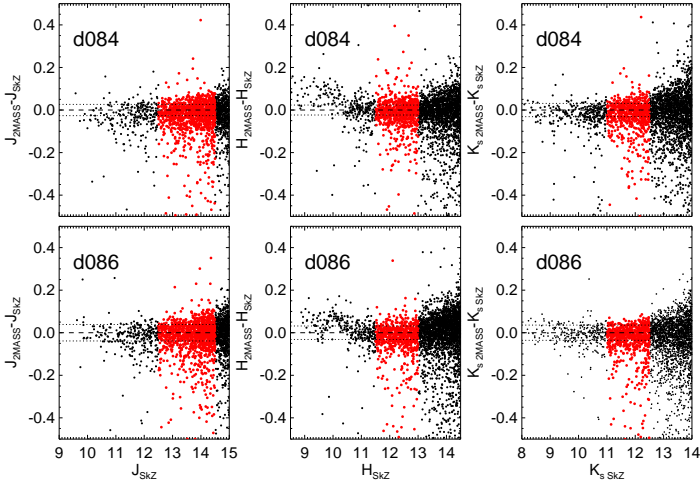


Fig. 2. Comparison between the VVV-SkZpipeline’s JHK_s photometry and the 2MASS catalog. Since the astrometry performed by the VVV-SkZpipeline is based on the 2MASS catalog, we could match most of the stars within a $1''$ -radius. Red, big circles are the stars within the magnitude intervals used for the flux calibration, i.e. $12.5 < J < 14.5$ mag, $11.5 < H < 13$ mag and $11 < K_s < 12.5$ mag. A dashed line shows where the VVV-SkZpipeline’s photometry matches perfectly the 2MASS values, and the dotted lines show the standard deviation of the points.

Danks 1 and Danks 2 were both present in VVV field d084, and RCW 79 was present in VVV field d086 (see Saito et al. 2012 for more details about VVV data). Those fields were acquired twice in the $ZYJHK_s$ bands on 7 to 29 March 2010, and 18 March to 4 April 2010, respectively, with the VIRCAM camera mounted on the VISTA 4m telescope at Paranal Observatory (Emerson & Sutherland 2010), and reduced at CASU² with the VIRCAM pipeline v1.1 (Irwin 2004). The total exposure time of each of these images was 40s, with 2 images per filter in average. For a detailed description of the observing strategy see Minniti et al. (2010). During the observations the weather conditions fell within all the survey constraints for seeing, airmass, and Moon distance (Minniti et al. 2010), and the quality of the data was satisfactory. JHK_s true color images of the three clusters are shown in Figure 1. Additional 8s K_s -band images were also obtained in order to find and monitor the variable stars in those fields. The dates, airmass, seeing, ellipticity and observation quality grade are all listed in Table 1 (see Online Material for complete version).

Stellar photometry was performed with the VVV-SkZpipeline (Mauro et al. 2012) automated software based on ALLFRAME (Stetson 1994) optimized for PSF photometry of VISTA data. Contrarily to the aperture photometry made available by CASU, the VVV-SkZpipeline is using single pointing images, called pawprints (covering 0.59 sq. deg), instead of the combination of 6 pawprints giving a full 1.64 sq. deg combined image, called tile (see Saito et al. 2012 for more details about pawprints and tiles). The reason for this is that sources on a tile have PSF shapes that are too difficult to model, due to the highly variable PSF across field-of-view of each combined pawprint. In these conditions, PSF fitting does not give much better accuracy than simple aperture photometry. To take into account for the variable PSF, the VVV-SkZpipeline simply has to allow the PSF to vary quadratically across the

pawprints’ field-of-view. The final product of the pipeline is an astrometric, flux calibrated star catalog. PSF photometry produces many spurious detections close to defects on the detectors, in the border of the fields, in the core and on the speckles of saturated stars, etc. Those can be isolated when, for all sources, the photometric errors given in the ALLFRAME’s output are compared with the magnitudes, since the error on the fit of those fake detections tends to be high. The VVV-SkZpipeline finds the maximum of the error distribution per magnitude bin (typically 0.1 mag), and fits a polynomial function to get the photometric error as a function of magnitude. We can then perform a sigma clipping, i.e. all detections showing a photometric error higher than 3σ are removed. One has to note that the errors given by ALLFRAME is not the real photometric error, since it does not take into account all the real sources of errors, like for instance the correlation of the noise of adjacent pixels in infrared detectors.

Stars brighter than $K_s \sim 12.5$ mag are saturated in the VVV disk area, but ALLFRAME uses the wings of the point-spread function of these stars and reaches an accuracy of 0.1 mag with stars up to mag=9.0. At the faint end, the same accuracy or better is achieved down to $J=20.0$ mag and $K_s=18.0$ mag. 2MASS photometry was used both for substituting the VVV photometry of stars brighter than $K_s=9.0$ mag and for absolute flux calibration. Flux calibration was done in the J -, H - and K_s -bands using stars with $12.5 < J < 14.5$ mag, $11.5 < H < 13$ mag and $11 < K_s < 12.5$ mag (see Figure 2). One has to note that the 2MASS photometry shows a dispersion higher than 0.1 mag for $K > 13$ mag. Since there is no reference in Z and Y in the 2MASS catalog, the pipeline simply corrects its output for the zero-point, giving an instrumental magnitude that is simply offset from the absolute value. Because the filters of VISTA and 2MASS are not identical, in addition to the zero point correction, we apply a color term to transform our catalogs into the 2MASS system. We preferred to apply this transformation rather than keeping the VISTA system, since most of the models we are using in this study and most of the other studies of massive clusters are made in the 2MASS system.

To calculate the completeness of our catalog, we created Luminosity Functions (LFs) for the clusters in bins of 0.5 K -band magnitudes. For each magnitude bin, we added artificial stars within the given magnitude ranges to the cluster image. The completeness was calculated by finding the recovery fraction of artificial stars per magnitude. The detection of the stars was done using DAOPHOT following a similar methodology as performed by the VVV-SkZpipeline.

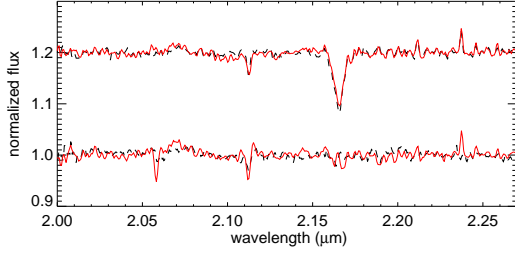
2.1.2. Field star decontamination

To disentangle field and cluster stars we adapted the statistical decontamination algorithm described in Bonatto & Bica (2010, and references therein) to exploit the VVV photometric depth in H and K_s (and related uncertainties). The first step requires the definition of a comparison field that, depending on the projected distribution of individual stars, clusters or clumpy extinction due to dark clouds in an image, may be a ring around the cluster or some other region selected in its immediate vicinity. The algorithm divides the full range of CMD magnitudes and colours into a grid of cells with axes along K_s , $(H - K_s)$ and $(J - K_s)$. Initial cell dimensions are $\Delta K_s = 1.0$ and $\Delta(H - K_s) = \Delta(J - K_s) = 0.2$ mag, but sizes half and twice those values are also considered, together with shifts in the grid positioning by $\pm 1/3$ of the respective cell size along the 3 axes. Thus, the number of independent decontamination outputs amounts to 729

² <http://casu.ast.cam.ac.uk/>

Table 1. Observation log. Columns include UT date, HJD-2.455e6, airmass, seeing in arcsec, ellipticity and quality grade provided by ESO. Both the d084 and d086 fields are presented. (see Online Material for complete version)

| VVV field d084 | | | | | | VVV field d086 | | | | | |
|----------------|-------------|-------|--------|------|-----|----------------|-------------|-------|--------|------|-----|
| UT Date | HJD-2.455e6 | AM | Sng | Ell. | QG | UT Date | HJD-2.455e6 | AM | Sng | Ell. | QG |
| 29 Mar 2010 | 284.092893 | 1.550 | 0.91'' | 0.05 | A | 23 Apr 2010 | 309.040379 | 1.552 | 0.67'' | 0.08 | A |
| 29 Mar 2010 | 284.093200 | 1.547 | 0.85'' | 0.06 | A | 23 Apr 2010 | 309.040738 | 1.548 | 0.69'' | 0.09 | A |
| 7 Apr 2010 | 293.088925 | 1.462 | 0.89'' | 0.08 | C | 11 May 2010 | 327.158628 | 1.269 | 0.76'' | 0.17 | C |
| ... | ... | ... | ... | ... | ... | ... | ... | ... | ... | ... | ... |

**Fig. 3.** Section of the K_s spectrum of two stars that were observed using different instruments and/or different slit masks. Obj2 (top) was observed with MMIRS using the first (solid, black line) and the second (dashed, red line) slit mask. Obj5 (bottom) was observed with NTT/SofI (solid, black line) and Clay/MMIRS (red, dashed line). An arbitrary shift in flux was applied for better visual representation.

for each cluster candidate. For each cell, the algorithm estimates the expected number density of member stars by subtracting the respective field star number-density³. Summing over all cells, each grid setup produces a total number of member stars N_{mem} and, repeating this procedure for the 729 different setups, we obtain the average number of member stars $\langle N_{\text{mem}} \rangle$. Each star is ranked according to the survival frequency after all runs, and only the $\langle N_{\text{mem}} \rangle$ highest ranked stars are taken as cluster members. Further details on the algorithm are described in Bonatto & Bica (2010). As a photometric quality constraint, the algorithm rejects stars with uncertainty in K_s and colours higher than 0.1 mag.

2.2. Near-infrared spectroscopy

2.2.1. Observations

We collected spectra of 6 and 8 stellar members of Danks 1 and Danks 2, respectively, using the infrared spectrograph and imaging camera SofI in long-slit mode on the New Technology Telescope (NTT) at La Silla Observatory ESO, Chile. Those stars are marked in Figure 1 by green circles. Using the medium resolution grism in the 3rd order, we covered the whole K_s -band, i.e. 2.00–2.30 μm , with a resolution of $\Delta\lambda=4.66 \text{ \AA}/\text{pix}$. We used a 1 arcsec slit, in order to match the seeing, which gives a resolving power of $R\sim 1320$. For optimal subtraction of the atmospheric OH emission lines, we used 60 arcsec nodding along the slit in an ABBA pattern, i.e. the star was observed before (A) and after (B) a first nod along the slit, then at position B a second time before returning to position A for a last expo-

sure. All stars were observed using two slit positions per cluster. The position angle of the slit was chosen so that two or more stars would be observed simultaneously. Total exposure time was 40s for Danks 1 star members, and 160s and 600s for the brightest and the faintest stars in Danks 2, respectively. The total signal-to-noise ratio (S/N) per pixel ranges from 60 for the faintest stars to 150 for the brightest ones. Bright stars of spectral type G were observed as a measure of the atmospheric absorption. Those stars were selected to share the same airmass as the targeted clusters' stars during the middle of their observation. The spectra of the two stars HD 113376 (G3 V) and HD 120954 (G1 V) were obtained after the observations of the first and the second slit position on Danks 1 on 14 and 18 April 2011, respectively. Also, the star HD 119550 (G2 V) was observed just after the two slit positions on Danks 2 on 15 April 2011.

We also obtained a total of 38 spectra of stars within, and in the vicinity of the star clusters Danks 1 and Danks 2 using the near-infrared spectrograph MMIRS in multi-object mode on the Clay telescope at Las Campanas Observatory on 2011 May 19–20. Those stars are marked in Figure 1 by red circles. Using the HK grism, we covered a spectral range of $\lambda\lambda = 1.25\text{--}2.45 \mu\text{m}$, with a resolution of $\Delta\lambda=6.70 \text{ \AA}/\text{pix}$. We needed two slit-mask designs to observe all our targets of interest. Both used a slit-width of 0.5 arcsec, which gives a resolving power of $R\sim 1120$. Similarly as for the SofI data, nodding along the slits was used, but due to the small size of the slits, we only used 2 arcsec nodding in an ABCCBA pattern (same as ABBA pattern, but involving a third position along the slit). Individual exposure time was limited to 300s to allow for accurate subtraction of the sky emission and the total exposure time was 2700s for all stars. The average total S/N per pixel reached ranges from 100 to 200 for stars brighter than $K_s = 12.0$ mag and from 30 to 90 for stars fainter than $K_s = 12.0$ mag. The star HD 114012 (spectral type A0 V) was observed after the first mask as a measure of the atmospheric absorption.

Martins et al. (2010) obtained great quality NIR spectra of stars in RCW79. Hence we use their spectra to complement our photometry.

2.2.2. Reduction and extraction

Before performing standard procedures for the reduction of the data, we had to take special care of certain aspects that are characteristic of the instruments we used. In the case of SofI spectra, we first had to correct for bad pixels, using the latest bad pixel mask available on the European Southern Observatory webpage⁴, and for cross-talk, as described in the SofI User's Manual (Moorwood et al. 1998). In the case of MMIRS spectra, a few more steps were needed. The data were obtained through

³ Photometric uncertainties are considered by computing the probability of a star of given magnitude and colour to be found in any cell (i.e., the difference of the error function computed at the cell borders).

⁴ http://www.eso.org/lasilla/instruments/sofi/tools/reduction/bad_pix.html

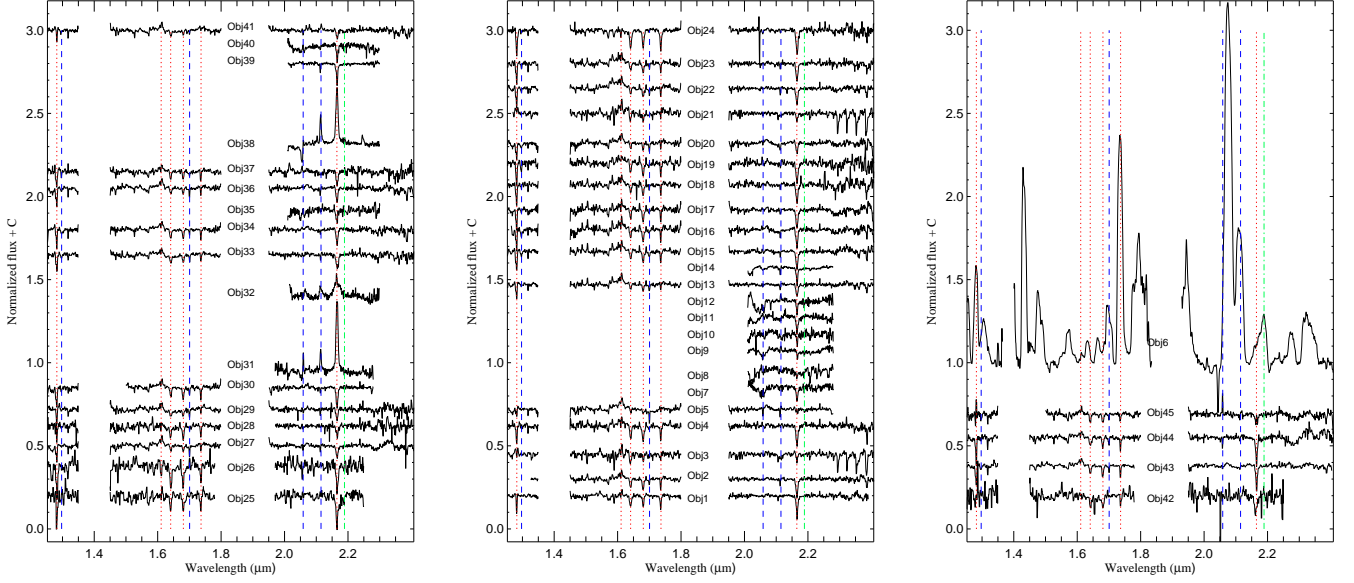


Fig. 4. Spectra of the stars in the area of the clusters Danks 1 (left), Danks 2 (middle) and DBS 132 (right). Obj6 (WC8 type) should be placed with the Danks 2’s spectra, but is presented in the right panel for better visibility. Hydrogen recombination lines are marked with vertical dotted, red lines and Helium lines with vertical dashed, blue lines.

“up the ramp” acquisition. Each fits file consists of a data cube containing the non-destructive readout of the whole detector at every 5s step. Hence, after subtracting the dark frame from the science data, one can collapse all readouts taken during an exposure into a single image by fitting a slope to the number of counts as a function of time for each pixel (as suggested on the MMIRS webpage⁵). By doing so, when the linearity and the saturation levels of each pixel are taken into account adequately, one corrects for cosmic rays and for saturated lines. The last step before running standard reduction was to find, trace and cut the individual slits in the original image. The traces were fitted using a 4th-order polynomial fit and rectified before being cut. All steps described above were executed using custom-written Interactive Data Language (IDL) scripts.

Subsequent nodding observations were subtracted from one another to remove bias level and sky emission lines. The flat fielding, spectrum extraction and wavelength calibration of all spectra were executed in the usual way using the IRAF⁶ software. Calibration lamp spectra (Xenon-Neon for SofI and Argon for MMIRS) taken at the beginning of each night were used for wavelength calibration. The wavelength solution of each frame has an r.m.s. uncertainty of ~ 0.5 pixels for SofI spectra and 0.2 pixels for MMIRS spectra, which correspond to ~ 30 and ~ 20 km s⁻¹, respectively. Correction for atmospheric absorption was done using the IRAF task *telluric*. When a G-type star was used, it was first divided by a solar spectrum downloaded from the National Solar Observatory (Livingston & Wallace 1991) and resampled following the method described by Maiolino et al. (1996). When an A0 star was used, we first subtracted a fitted Voigt profile from the standard Br absorption features before running the task *telluric*. Finally, all spectra were rectified using a low-order polynomial fit to a wavelength interval that

was assumed to be pure continuum, i.e. where no absorption or emission lines were observed nor expected. Unfortunately, due to bad weather, the observing night was abruptly interrupted just before we could observe a telluric standard for the second mask at Las Campanas. Both masks were observed during different nights, but since they were observed at comparable airmass (~ 1.2), we decided to use the same telluric standard for all spectra. Depending on how the weather conditions and the sky level were different during the two nights, this could have introduced uncertainties in the extraction of the spectra of the second mask, but nothing significant is observed. Indeed, one star was observed with both masks and, as one can see in Figure 3 where is shown a comparison of the two spectra, they are very similar. Figure 3 also shows the similarity of two spectra of another star observed using both SofI and MMIRS. Hence our reduction and extraction methods can be trusted.

2.2.3. Spectral classification

The spectra of the stars in the area of the clusters Danks 1, Danks 2 and DBS2003 132 are plotted in Figure 4. The preliminary raw spectral classification was done using available catalogs of *K*-band spectra of objects with spectral types derived from optical studies (Morris et al. 1996; Figer et al. 1997; Hanson et al. 1996, 2005) as well as the spectral catalogs of Martins & Coelho (2007), Crowther et al. (2006), Liermann et al. (2009), Mauerhan et al. (2011) and Davies et al. (2012). The most prominent lines in our wavelength range are Br γ (4–7) $2.1661 \mu\text{m}$, Br 10 (4–10) $1.737 \mu\text{m}$, Br 11 (4–11) $1.681 \mu\text{m}$ and Br 12 (4–12) $1.641 \mu\text{m}$ (from the Brackett series), Pa β (3–5) $1.282 \mu\text{m}$ (from the Paschen series), HeI lines at $2.1127 \mu\text{m}$ ($3p^3P^o - 4s^3S$, triplet), $1.702 \mu\text{m}$ ($1s^4d^3D^o - 1s^3p^3P^o$), $1.668 \mu\text{m}$ (4–11) and $1.722 \mu\text{m}$ (4–10), HeII lines at $2.188 \mu\text{m}$ (7–10) and $1.692 \mu\text{m}$ (12–7), the blend of CIII, NIII and OIII at $2.115 \mu\text{m}$, NIII $\lambda 2.103 \mu\text{m}$, and CII lines at $2.070 \mu\text{m}$ and $2.079 \mu\text{m}$. All those lines were compared with the template spectra from these papers.

⁵ <http://hopper.si.edu/wiki/mmti/MMTI/MMIRS/MMIRS+Pipeline>

⁶ IRAF is distributed by the National Optical Astronomy Observatories (NOAO), which is operated by the Association of Universities for Research in Astronomy, Inc. (AURA) under cooperative agreement with the U.S.A. National Science Foundation (NSF).

The Equivalent Widths (EWs) of Danks 1, Danks 2 and DBS 132 of the Br 11 (4–11) and HeI 1.702 μm lines of the spectral targets were measured on the continuum normalized spectra, by the IRAF task *splot*. In general, we are using a Gaussian profile fitting with a linear background, in more complicated profiles we used the deblending function or Voigt profile fitting. The EW uncertainties were estimated taking into account the S/N of the spectra, the peak to continuum ratio of the line (see Bik et al. 2005) and the error from the telluric star subtraction (which was estimated to be $\sim 10\text{--}15\%$ in the worst cases). The EWs of the emission lines are negative by definition. Their ratio was used for qualitative estimation of the spectral types of OB stars using the calibrations given in Hanson et al. (1998). In general, the spectra of most stars show the HeI lines and the Brackett series in absorption, which is typical for O and early B main sequence (MS) stars; several stars namely Objs. 1, 4, 19, 25, 26, 28, 42 show only Brackett series in absorption and are classified as later B - early A type stars. The stars Obj 3 and 21 present CO, MgI, Fe, Ca and AlI lines, characteristic of late type stars. Obj 3 was reported by Davies et al. (2012, their number D2-2) and classified as F8/G1, but they concluded that the star was foreground from its near-infrared colors. We assign G7/8 I spectral type to Obj 21 based on comparison with template spectral library of Rayner et al. (2009). Objs. 6, 31, 32, 38 are WR stars previously discovered by Davies et al. (2012, their numbers D2-3, D1-1, D1-5 and D1-2, respectively) and Mauerhan et al. (2011, their numbers MDM8 and MDM7). The adopted spectral types are given in Table 2. This method of spectral classification, especially in the near-IR is correct within 2 subtypes, thus we adopted this error for our estimates.

3. Results

In this section we describe our methods to determine the fundamental parameters of the young massive clusters, such as the angular size, RV, extinction, distance, age, and mass.

3.1. Angular size

One parameter that can be directly determined is the angular radius of the clusters. We first get the coordinates of the cluster center, based on our stellar catalog. Starting from a first-guess value, we calculated the radial density profile (RDP) iteratively until we converged towards to best profile. Using this method, we get:

$$\begin{aligned} \text{Danks 1 : RA(J2000)} &= 13 : 12 : 26.74 \\ \text{DEC(J2000)} &= -62 : 41 : 37.81 \\ \text{Danks 2 : RA(J2000)} &= 13 : 12 : 55.14 \\ \text{DEC(J2000)} &= -62 : 40 : 52.00 \\ \text{RCW 79 : RA(J2000)} &= 13 : 40 : 11.27 \\ \text{DEC(J2000)} &= -61 : 43 : 52.10 \end{aligned}$$

Once the converged RDP is obtained (see results in Figure 5), we evaluate the stellar density of the field stars in the vicinity of the clusters. For better guiding our determination of the angular size of the clusters, we fit a 2-parameter King profile adapted to star-counts (same as King 1966, but using star-counts instead of surface brightness). The 2 parameters are the projected central density of stars (S_0) and the core radius (r_c). The uncertainties on the fit are given by the maximum and minimum values allowed within the error bars of the data points (given by Poissonian noise).

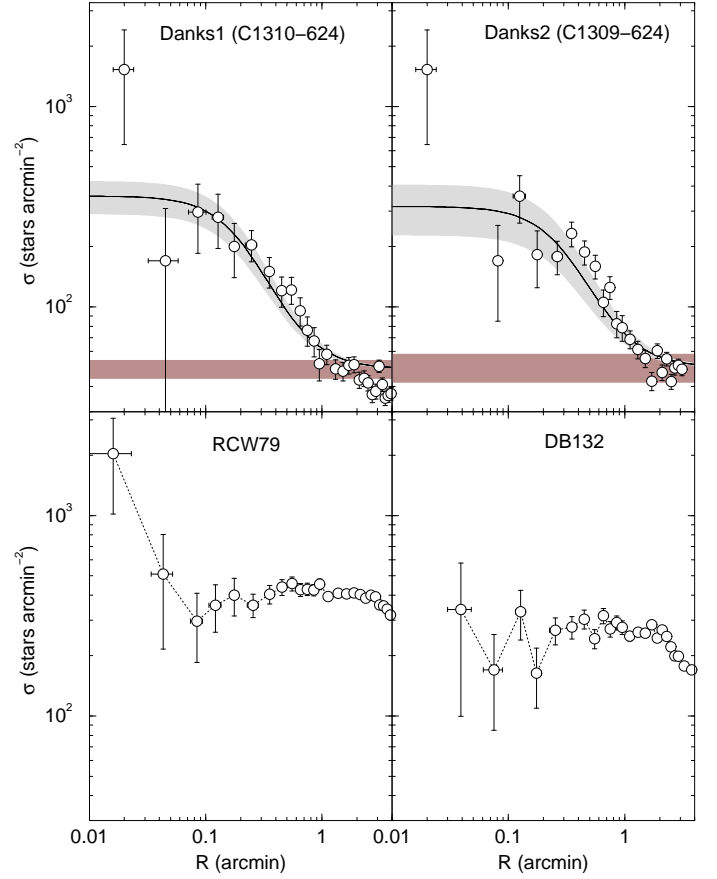


Fig. 5. Radial density profiles for Danks 1, Danks 2 and RCW 79. The error bars are given by Poissonian noise, the solid line shows the fit of a 2-parameter King profile (with uncertainties plotted in gray) and the purple rectangle gives the field density level. Unfortunately, no fit was possible for RCW 79 and DBS 132.

The angular size is defined where the RDP meets the level of the field stars. An angular size of 1.5 ± 0.5 arcmin is found for both Danks 1 and Danks 2. We get $S_0 = 308 \pm 54$ stars/arcmin² and $r_c = 0.21 \pm 0.03$ for Danks 1, and $S_0 = 267 \pm 98$ stars/arcmin² and $r_c = 0.32 \pm 0.06$ for Danks 2. RCW 79 does not follow a typical cluster profile. This could be due to artifacts, since bright saturated stars leave big holes in the catalog where the star count is artificially deficient. On the other hand, King profiles are meant to describe relaxed globular clusters, not young open clusters, RCW 79 shows a quite irregular form. Other profiles were also used, but with meaningless results. Still, it shows a stellar density excess at radius $R < 0.1$ arcmin that appears to reach $R \sim 1$ arcmin, hence we can use this value as our estimate of the angular size. As for DB132, the stellar RDP is flat up to $R \sim 3$ arcmin and is not typical for a cluster.

3.2. Memberships of the spectral targets and RVs

The spectroscopic targets were selected using statistically decontaminated CMDs (Bonatto & Bica 2010). During the observations however, some additional stars fell in the slits and it is well known that the statistical decontamination method is far from perfect with respect to the cluster membership. The ideal solution to the problem is to calculate the proper motions of the stars in the region. Unfortunately the VVV database at the mo-

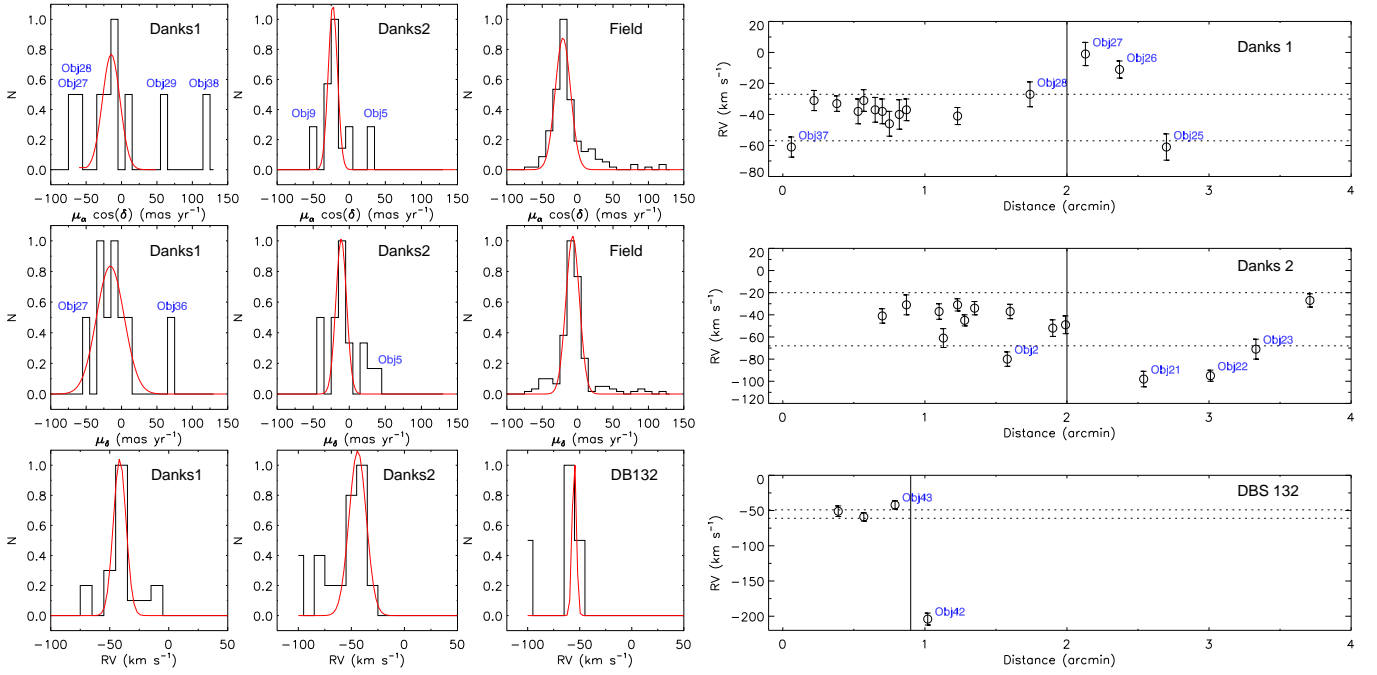


Fig. 6. Left: Top and middle panel: Histograms and proper motion distributions of $\mu_\alpha \cos \delta$ and μ_δ of Danks1, Danks2 and comparison field. Left: Bottom panel: RV distributions of Danks1, Danks2 and DB132. The solid lines represent the best Gaussian fit, outliers are labeled. Right: Radial velocities for our spectroscopic targets as a function of distance from the Danks 1 (top), Danks 2 (middle) and DBS 132 (bottom) cluster centers. The horizontal lines represent the dispersion of the Gaussian fit (see text). The adopted cluster diameter is shown by the vertical line. The error bars represent the random error in determining the RV for each star.

ment contains observations for two years only and is insufficient to determine precise proper motions at this point.

Thus, we built the proper motion histograms using the absolute proper motions from the PPMXL Catalog of Positions and Proper Motions on the ICRS (Roeser et al. 2010). At the distance of Danks 1 and 2 (3–4 kpc, Davies et al. 2012, this work) the absolute proper motions are not very accurate (the mean error of the sample is ~ 9 mas), but nevertheless can be used for some estimates (with 40–50% accuracy). Unfortunately, only 9 spectroscopic targets of Danks1 and 18 of Danks 2 are available for analysis. The corresponding proper motion distribution histograms are shown in Figure 6, together with the proper motion distribution of comparison field (RA = 198.35231 and DEC = -62.826599). Using the Bonatto & Bica (2011) algorithm we fitted the distributions with a Gaussian profile, which provides the velocity dispersions (σ) and the average velocity (μ) of the stars. They are given in Table 3. Stars outside the 5σ limit of the fit are considered field stars. Such a conservative limit is justified by the large errors of the proper motions.

On the other hand, the RVs of the spectral targets also can be used to check the membership. In this case we measured the RV using the IRAF task *rvidlines* which fits spectral lines to determine the wavelength shift with respect to specified rest wavelengths. For this procedure, we used as many H α and H β lines as available in the spectra (typically 7–10 lines per spectrum), and we reach an accuracy equivalent to more or less a tenth of a resolution element, i.e. typically ~ 20 km s $^{-1}$. As in the proper motion analysis we fitted the RV distribution histogram with a Gaussian function. Then we plotted the RV as a function of distance from the Danks 1, Danks 2 and DBS 132 cluster centers (Figure 6, bottom left and right panels) and analyzed the stars outside the dispersion lines of the Gaussian fit distributions. Dashed lines correspond to the 3σ interval, and any star

outside those limits is considered field star. Objs 27 and 28 from Danks 1 can be immediately classified as field stars, while Obj 37 (also observed by Davies et al. 2012, their number D1-12) has a peculiar RV, but its spectrum implies cluster membership. The RV of Danks 2 are much more homogeneous, without obvious outliers. For DBS 132, Obj 42 has a RV that is much higher than the dispersion interval so that it is most probably a field star. One should note that this analysis is based on a single epoch observation and follow-up observations of other epochs would be needed to eliminate bias due to binarity, especially since the binary fraction among OB and WR stars is high ($f_{bin} > 0.5$ for OB stars; Sana et al. 2011 and references therein; and $f_{bin} \sim 0.4$ for WR stars; Schnurr et al. 2008 and references therein). Average RV of the clusters are listed in Table 3. One can see that they are consistent with $v_{LSR} = -39.4$ km s $^{-1}$ (see Davies et al. 2012, Figure 7). Also, Danks 1 and Danks 2 have the same RV, which indicates that they are binary clusters. The value for DBS 132 is significantly larger than for the Danks' clusters, but it is based on only 3 stars. Note that similar analysis of the RVs has been done for RCW 79 by Martins et al. (2010), hence it is not repeated here.

The last check that we performed was to analyze the position of the stars in the $J - K_s$ vs. K_s CMD. Objs 25, 34, 40 and 41 (Danks 1) and Objs 1, 3, 10, 14 and 21 (Danks 2) have peculiar positions in the diagram, far from the MS and the sequence of evolved stars. Of course, this could be due to differential reddening (see discussion in the next section). We attempted to reduce the effect of differential reddening by employing the reddening-free parameter $Q_{IR} = (J - H) - 1.70(H - K_s)$, as defined by Negueruela et al. (2007) for OB stars (see also Catelan et al. 2011 for a list of several other reddening-free indices in the $ZYJHK$ system). We chose this parameter to avoid the intrinsic degeneracy between reddening and spectral type (and since

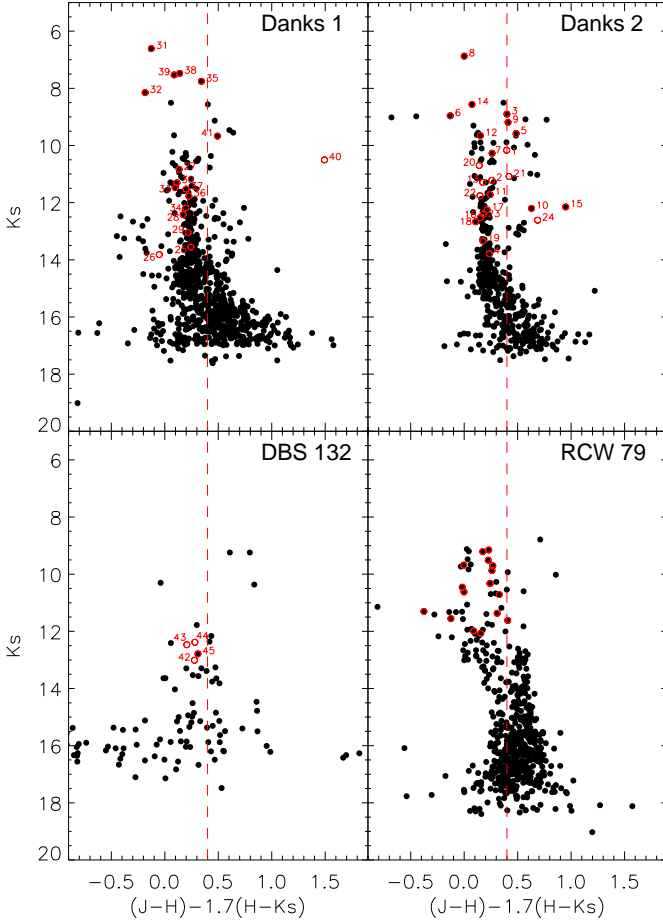


Fig. 7. Reddening free color of $(J - H) - 1.70(H - K_s)$, also called Q_{IR} plotted vs. K_s magnitude. Red circles mark the stars for which spectra have been observed, and the number attached to them refers to the name of the star listed in Table 2. The red, vertical dashed line is placed at $Q_{IR} = 0.4$ (see text for more details).

we expect to find early OB stars in the majority of the clusters in our sample). Figure 7 shows this reddening free parameter vs. K_s magnitude. Originally, Negueruela et al. (2011) defined $Q_{IR} \leq 0.0-0.1$ as a separating value for early-type stars. Later on Ram rez Alegr a et al. (2012) and Borissova et al. (2012) defined the separation value for OB stars as $Q_{IR} \leq 0.3-0.4$. Indeed, plotting our objects in the reddening free diagrams, most probably Obj 25 and 34 are affected by differential reddening, while Objs 40 and 41 show infrared excess and are situated far from the standard OB sequence on this diagram. The Objs 1, 3, 15, 21 and 24 of Danks 2 occupy peculiar positions on the reddening free CMD. The Obj 3 was observed and classified by Davies et al. (2012, their number D2-2) as a yellow supergiant (F8-G3 I). It is hard to say if the object is a cluster member or not. The radial velocity of the object is bigger than the mean value of the cluster (-61 km/s), but the error is large ± 17 km/s, the proper motion values are also relatively far from the mean value. Most probably is a field star, as classified by Davies et al. (2012). If not, it will be another case of simultaneous population of supergiant and WR stars in the same cluster. But, to verify its status accurate proper motion measurements are necessary. The Objs 1, 10, 21 and 24 are most probably field stars. For DBS 132 and

RCW 79 all spectroscopically observed targets occupied the expected region of OB stars.

The reddening free CMDs can be used to separate the MS from the pre-main sequence (PMS) stars. In all cases, except for DBS 132 the PMS population is well separated, and can be defined as stars with $Q_{IR} > 0.4$ and $K_s > 14$; $K_s > 15$; $K_s > 14$ and $K_s > 13$ mag for Danks 1, Danks 2, DBS 132, and for RCW 79, respectively. This separation was used during the isochrone fitting and mass calculation.

3.3. Extinction

The new spectroscopic classifications and infrared observations permit the extinction and reddening laws to be evaluated directly for dust along the line-of-sight, thereby mitigating the propagation of uncertainties. The extinction and reddening laws are known to vary throughout the Galaxy. For example, Turner (2011) noted that dust in the direction of the η Car complex follows an anomalous extinction and reddening law. A variable extinction analysis (e.g. Turner 1976, Majaess et al. 2011) may be employed to evaluate both the ratio of total-to-selective-extinction, e.g., $A_{K_s}/E(J - K_s)$, for the line-of-sight and the distance to Danks 1 and Danks 2. Sizable statistics are required for the analysis, and thus the clusters were assumed to lie at the same distance. That assumption is supported by the new RVs derived here and the results of Davies et al. (2012). From the expression for computing the distance to a star we get:

$$K_s - M_{K_s} - R_{K_s} \times E(J - K_s) = 5 \times \log d - 5, \quad (1)$$

where we define $R_{K_s} = A_{K_s}/E(J - K_s)$. The equation simplifies for a cluster of stars at a common distance. Rearranging Equation (1) yields:

$$(K_s - M_{K_s}) = R_{K_s} \times E(J - K_s) + \text{const.} \quad (2)$$

A determination of R_{K_s} and $5 \times \log d - 5$ follows from correlating $K_s - M_{K_s}$ and $E(J - K_s)$. M_{K_s} and $E(J - K_s)$ were inferred from the new spectroscopic observations for stars in Danks 1 and Danks 2. Intrinsic parameters from Schmidt-Kaler (1982) and Koornneef (1983) were adopted. A least squares fit to the data yields $d = 3.6 \pm 0.5$ kpc and $R_{K_s} = 0.60 \pm 0.24$. The results established favor the larger distance to Danks 1 and Danks 2 proposed by Davies et al. (2012). The topic is elaborated upon in the next section.

The value of A_{K_s} was subsequently tabulated using the ratio derived above. The averages derived from all cluster members are $A_{K_s} = 1.11 \pm 0.24$ mag and $A_{K_s} = 0.88 \pm 0.34$ mag for Danks 1 and Danks 2 respectively. The results agree with those determined by Davies et al. (2012), to within the uncertainties. For DBS 132 we calculated $A_{K_s} = 1.30 \pm 0.34$ mag. We did not obtain spectra of RCW 79's members, but adopting the spectral classification of the stars observed by Martins et al. (2010), we get $A_{K_s} = 0.56 \pm 0.04$ mag. The errors represent only the standard deviation from the mean value and can be relatively large in some cases, suggesting differential extinction. As can be seen from Table 2 however, in the case of Danks 2, only one star has a large reddening value of $A_{K_s} = 2.16$ mag, namely Obj 14, which exhibits peculiar behavior. Excluding this star from the calculation we get a much smaller error on the mean

Table 2. Position, photometry and spectral parameters. Columns include the name of the star, the Davies et al. (2012, hereafter D12) identification number, the right ascension (RA), the declination (DEC), V (taken from Baume et al. 2009), J , H and K_s photometry (in mag), the RV, the spectral type (determine from comparison with template spectra and UBV photometry), extinction (A_K) and distance (d), respectively. Stars are ordered as a function of their (non-)membership.

| name | D12 name | RA (J2000) | DEC (J2000) | V | J | H | K_s | RV (km s ⁻¹) | Sp. Typ. | A_K (mag) | d (kpc) |
|--------------------------------|-------------|---------------|----------------|-------|-------|-------|-------|-----------------------------|----------|----------------|------------|
| <i>Danks 1 field stars:</i> | | | | | | | | | | | |
| Obj25 | | 13 12 36.310 | -62 41 22.60 | 23.07 | 15.41 | 14.15 | 13.55 | -61±17 | B9/A0V | 1.14±0.05 | 2.50 |
| Obj26 | | 13 12 35.290 | -62 41 53.71 | 20.49 | 15.34 | 14.40 | 13.82 | -11±11 | B9/A0V | 0.93±0.03 | 3.11 |
| Obj27 | | 13 12 34.156 | -62 41 36.01 | 18.23 | 12.08 | 11.24 | 10.83 | -1±15 | B2/3V | 0.82±0.04 | 2.15 |
| Obj28 | | 13 12 32.760 | -62 42 07.61 | 20.43 | 13.99 | 12.94 | 12.42 | -27±16 | B9/A0V | 0.96±0.03 | 1.61 |
| Obj29 | | 13 12 30.240 | -62 41 29.40 | 20.85 | 14.46 | 13.49 | 13.05 | -41±11 | B2/3V | 0.92±0.04 | 5.71 |
| Obj40 | | 13 12 23.234 | -62 42 01.00 | 20.23 | 12.22 | 10.59 | 10.50 | -37±16 | O9/B0V | 1.15±0.03 | 3.56 |
| Obj41 | D1-8 | 13 12 22.879 | -62 41 48.83 | 18.64 | 11.27 | 10.08 | 9.67 | -31±14 | O4-6 | 1.08±0.03 | 4.04 |
| <i>Danks 1 members:</i> | | | | | | | | | | | |
| Obj30 | | 13 12 29.299 | -62 42 07.12 | 21.66 | 12.67 | 11.77 | 11.31 | -37±14 | B2/3V | 0.89±0.06 | 2.60 |
| Obj31 | D1-1 | 13 12 28.560 | -62 41 43.80 | 14.96 | 8.26 | 7.27 | 6.61 | -46±16 | WNLh | | |
| Obj32 | D1-5 | 13 12 28.517 | -62 41 51.00 | 16.21 | 9.81 | 8.83 | 8.15 | -38±16 | WNLh | | |
| Obj33 | | 13 12 28.061 | -62 42 08.23 | 19.29 | 12.84 | 11.95 | 11.48 | -31±14 | B2/3V | 0.89±0.06 | 2.81 |
| Obj34 | | 13 12 27.459 | -62 41 19.27 | 21.41 | 13.99 | 12.78 | 12.19 | -40±19 | B2/3V | 1.16±0.07 | 3.45 |
| | D1-7 | 13 12 26.800 | -62 41 56.36 | 18.16 | 10.78 | 8.70 | 8.14 | | O4-6 I | 1.74±0.03 | 2.42 |
| | D1-11 | 13 12 26.320 | -62 42 05.78 | 18.99 | | | | | O8-B3 V | | |
| | D1-6 | 13 12 26.220 | -62 42 09.37 | 16.36 | 9.91 | 9.01 | 8.51 | | O6-8If | 0.99±0.04 | 4.06 |
| Obj35 | D1-4 | 13 12 26.218 | -62 41 57.90 | 16.95 | 9.61 | 8.32 | 7.76 | | O6-8If | 1.26±0.03 | 2.53 |
| Obj36 | | 13 12 26.107 | -62 41 39.89 | 20.14 | 13.20 | 12.22 | 11.77 | -33±10 | B2/3V | 0.93±0.06 | 3.16 |
| | D1-9 | 13 12 26.020 | -62 42 15.59 | 19.01 | 11.34 | 10.28 | 9.69 | | O4-6 | 1.11±0.03 | 4.01 |
| Obj37 | D1-12 | 13 12 25.690 | -62 42 05.17 | 19.39 | 12.83 | 11.93 | 11.53 | -61±13 | B2/3V | 0.86±0.04 | 2.92 |
| Obj38 | D1-2 | 13 12 25.006 | -62 42 00.21 | 17.40 | 9.422 | 8.15 | 7.48 | -31±13 | WNLh | | |
| | D1-10 | 13 12 24.500 | -62 42 08.52 | 19.39 | 12.10 | 10.10 | 10.43 | | O4-6 | 1.25±0.03 | 5.63 |
| Obj39 | D1-3 | 13 12 23.748 | -62 42 01.37 | 17.36 | 9.41 | 8.20 | 7.53 | -38±16 | O7/8I | 1.28±0.03 | 2.26 |
| <i>Danks 2 field stars:</i> | | | | | | | | | | | |
| Obj1 | | 13 13 11.340 | -62 41 10.68 | 12.25 | 10.62 | 10.19 | 10.17 | -41±12 | B9/A0V | 0.28±0.05 | 0.78 |
| Obj2 | | 13 13 00.840 | -62 39 54.66 | 17.92 | 12.32 | 11.53 | 11.22 | -80±13 | B3/4V | 0.73±0.06 | 2.40 |
| Obj3 | D2-2 | 13 12 59.986 | -62 40 40.16 | 12.19 | 9.61 | 9.01 | 8.90 | -61±17 | F8-G1 | | |
| Obj10 | | 13 12 56.112 | -62 40 53.90 | 16.41 | 14.42 | 12.79 | 12.20 | | B2/3V: | 1.41±0.06 | 3.09 |
| Obj21 | | 13 12 45.300 | -62 40 42.16 | 18.43 | 12.61 | 11.50 | 11.08 | -98±14 | G7/8I | | |
| Obj22 | | 13 12 43.459 | -62 40 57.40 | 18.22 | 12.87 | 12.12 | 11.76 | -95±10 | B5/6V | 0.72±0.05 | 2.21 |
| Obj23 | | 13 12 42.250 | -62 41 11.42 | 19.80 | 13.65 | 12.79 | 12.40 | -71±18 | B5/6V | 0.80±0.07 | 2.85 |
| Obj24 | | 13 12 41.290 | -62 41 51.40 | 20.15 | 13.72 | 12.77 | 12.62 | -27±12 | B3/4V | 0.73±0.07 | 4.56 |
| <i>Danks 2 members:</i> | | | | | | | | | | | |
| Obj4 | | 13 12 58.930 | -62 40 46.49 | 19.32 | 15.05 | 14.17 | 13.79 | -31±18 | B8/9V | 0.78±0.04 | 3.81 |
| | D2-7 | 13 12 58.560 | -62 40 54.84 | 16.73 | 10.76 | 9.95 | 9.56 | | O4/6V | 0.84±0.05 | 4.75 |
| Obj5 | D2-6 | 13 12 58.351 | -62 40 37.34 | 19.60 | 10.86 | 10.04 | 9.63 | | O8/9V | 0.85±0.04 | 3.37 |
| Obj6 | D2-3 | 13 12 57.739 | -62 40 59.91 | 17.25 | 10.83 | 9.83 | 9.88 | | WC7-8 | | |
| Obj7 | | 13 12 57.737 | -62 40 40.13 | 17.58 | 11.50 | 10.63 | 10.27 | | O9/B0V: | 0.85±0.03 | 3.67 |
| | D2-9 | 13 12 57.083 | -62 40 00.49 | | 15.19 | 13.42 | 12.64 | | O6-8 | | |
| Obj8 | D2-1 | 13 12 56.419 | -62 40 28.43 | 14.79 | 8.30 | 7.40 | 6.87 | | O8-B3I | 1.00±0.04 | 1.90 |
| Obj9 | D2-4 | 13 12 56.266 | -62 40 51.24 | 16.41 | 10.47 | 9.51 | 9.19 | | O6/7 V | 0.89±0.05 | 3.53 |
| Obj11 | | 13 12 54.871 | -62 41 03.96 | 18.73 | 12.89 | 12.06 | 11.72 | | B2/3V: | 0.77±0.06 | 3.32 |
| Obj12 | D2-5 | 13 12 54.485 | -62 41 05.01 | 16.62 | 10.80 | 10.02 | 9.65 | | O7/8V | 0.81±0.03 | 4.09 |
| | D2-8 | 13 12 54.370 | -62 40 45.48 | 16.80 | 11.14 | 10.34 | 9.92 | | O6-8V | 0.84±0.05 | 3.87 |
| Obj13 | | 13 12 52.730 | -62 40 54.51 | 17.93 | 12.41 | 11.64 | 11.29 | -41±13 | B0/1V | 0.77±0.07 | 4.91 |
| Obj14 | | 13 12 51.773 | -62 39 55.96 | 18.75 | 11.91 | 9.78 | 8.57 | -31±11 | O7/8I | 2.16±0.03 | 2.43 |
| Obj15 | | 13 12 51.221 | -62 41 02.38 | 19.43 | 13.17 | 12.18 | 12.15 | -37±14 | B3/4V | 0.68±0.06 | 3.76 |
| Obj16 | | 13 12 50.541 | -62 40 22.86 | 19.54 | 13.72 | 12.91 | 12.53 | -45±10 | B5/6V | 0.76±0.07 | 3.08 |
| Obj17 | | 13 12 50.160 | -62 41 00.96 | 18.85 | 13.41 | 12.60 | 12.26 | -34±12 | B5/6V | 0.74±0.07 | 2.75 |
| Obj18 | | 13 12 49.159 | -62 41 00.20 | 19.39 | 13.82 | 13.05 | 12.67 | -37±13 | B5/6V | 0.74±0.07 | 3.32 |
| Obj19 | | 13 12 48.130 | -62 41 13.36 | 19.88 | 14.44 | 13.68 | 13.34 | -52±15 | B7/8V | 0.69±0.13 | 3.71 |
| Obj20 | | 13 12 47.520 | -62 40 54.48 | 17.40 | 11.82 | 11.06 | 10.60 | -49±16 | B0/1V | 0.77±0.07 | 3.74 |
| <i>DBS2003 132 field star:</i> | | | | | | | | | | | |
| Obj42 | | 13 12 22.270 | -62 42 38.28 | 22.05 | 14.70 | 13.53 | 13.01 | -204±17 | B7/8V | 1.04±0.13 | 2.49 |
| <i>DBS2003 132 members:</i> | | | | | | | | | | | |
| Obj43 | | 13 12 21.004 | -62 41 48.41 | 20.78 | 13.98 | 12.95 | 12.47 | -42±12 | B5/6V | 0.96±0.07 | 2.87 |
| Obj44 | | 13 12 19.871 | -62 42 25.23 | 23.02 | 14.41 | 13.03 | 12.38 | -51±15 | B3/4V | 1.30±0.06 | 3.35 |
| Obj45 | | 13 12 16.202 | -62 42 10.20 | 21.06 | 15.39 | 13.64 | 12.79 | -59±12 | B3/4V | 1.64±0.06 | 3.44 |

value and $A_{K_s} = 0.80 \pm 0.08$ mag for Danks 2. The reddening of DBS 132 is calculated using only 3 spectroscopically observed stars, but the color spread of DBS 132's cluster CMDs (see below) is ~ 1 mag, hence much larger than the typical photometric errors, also suggesting large differential extinction. The color spread is ~ 0.4 mag and ~ 0.3 mag in Danks 1 and RCW 79, which is much smaller than in DBS 132, but still significant.

The mean color-excess inferred for stars in Danks 2 is: $E(J - K_s) = 1.21 \pm 0.02(\sigma_{\bar{x}}) \pm 0.09(\sigma)$ mag, $E(J - H) = 0.85 \pm 0.02(\sigma_{\bar{x}}) \pm 0.07(\sigma)$ mag and $E(B - V) = 2.40 \pm 0.06(\sigma_{\bar{x}}) \pm 0.24(\sigma)$ mag, where σ is the standard deviation and $\sigma_{\bar{x}}$ is the standard error, i.e. σ divided by the square root of the sample size. The aforementioned mean reddenings were inferred from the intrinsic *BVJH* colors of Turner (1989) and Straizys & Lazauskaitė (2009), namely to provide an independent check on the extinction estimates determined from the intrinsic parameters of Schmidt-Kaler 1982 and Koornneef 1983 in the preceding paragraph. The mean color excess inferred from the spectroscopic observations for stars in Danks 1 is: $E(J - K_s) = 1.63 \pm 0.05(\sigma_{\bar{x}}) \pm 0.21(\sigma)$, $E(J - H) = 1.07 \pm 0.04(\sigma_{\bar{x}}) \pm 0.15(\sigma)$ and $E(B - V) = 2.68 \pm 0.06(\sigma_{\bar{x}}) \pm 0.27(\sigma)$. Dust emission observed in WISE images of the field support the finding that Danks 1 suffers additional obscuration relative to Danks 2.

Baume et al. (2009) discovered that the canonical reddening law does not characterize dust associated with the target clusters. The ratio $E(J - H)/E(H - K_s)$ may be inferred from all stars observed along the line of sight. A median (after making a $1.5\sigma_{\bar{x}}$ clip) yields $E(J - H)/E(H - K_s) = 2.20 \pm 0.06(\sigma_{\bar{x}}) \pm 0.37(\sigma)$, which is far in excess of the various values for the inner Galaxy listed in Table 1 of Straizys & Lazauskaitė (2008)'s work. It is also larger than the values tabulated in Majaess et al. (2011) and Majaess et al. (2012). The results imply that the line-of-sight $\ell \sim 305^\circ$ exhibits an anomalous reddening law, thus corroborating Baume et al. (2009) prior findings. The average *JHK_s* reddening law for the inner Galaxy is $E(J - H)/E(H - K_s) \sim 2.0$ (Straizys & Lazauskaitė 2009), and Majaess et al. (2011) noted that $E(J - H)/E(H - K_s) \sim 1.94$ appears to describe dust in the field of the classical Cepheid TW Nor. The region encompassing Danks 1 and Danks 2 was not surveyed by Straizys & Lazauskaitė (2009) in their analysis of the reddening law throughout the inner Galaxy. The ratio $E(B - V)/E(J - H)$ derived from the data likewise differs from the canonical value (see also Baume et al. 2009). The reddening law determined was subsequently employed to interpret the *JHK_s* CMDs. An evaluation of the ratio of total to selective extinction and reddening law in the optical ($E(U - B)/E(B - V)$, R_V) did not yield viable results, presumably since the uncertainties are magnified owing to the added temperature sensitivity of optical passbands and uncertainties tied to acquiring solid *U*-band photometry (a challenge).

A decontaminated *J - H* vs. *H - K_s* CCD is presented in Figure 8. O and B stars are marked with blue and orange circles, respectively. The intrinsic colors of the MS stars and giant branch (Koornneef 1983) are plotted using blue dashed lines. The reddening vector determined above is plotted in orange. Sources located to the right and below the reddening line may have excess emission in the near infrared (IR-excess sources) and/or may be PMS stars.

In this paper we will use $A_{K_s} = 1.11 \pm 0.24$, $A_{K_s} = 0.88 \pm 0.34$ mag, $A_{K_s} = 1.30 \pm 0.34$ mag and $A_{K_s} = 0.56 \pm 0.04$ mag for Danks 1, Danks 2, DBS 132 and RCW 79, respectively. The results are tied to the intrinsic parameters of Schmidt-Kaler 1982 and Koornneef 1983, since R_{K_s} was derived using those studies. Straizys & Lazauskaitė 2009 supply intrinsic colors only. To

within the uncertainties, the parameters derived are consistent using either dataset.

3.4. Distances

The distances to the stars for which we have obtained spectra were calculated and are presented in Table 2. The extinction and M_K values determined in the previous section were used to get the distance modulus. For each cluster, we select the star members for which we are confident of the spectral type. Hence, we get distances of $(m - M)_0 = 12.7 \pm 0.6$ mag (3.5 ± 1.0 kpc, 8 stars, dwarfs only, namely: Objs 30, 33, 34, 36, 37, 40, 4, D1-10), $(m - M)_0 = 12.8 \pm 0.5$ mag (3.7 ± 0.5 kpc, 15 stars, dwarfs only, namely: Objs 4, 5, 7, 9, 11, 12, 13, 15, 16, 17, 18, 19, 20, D2-8, D2-7), $(m - M)_0 = 12.5 \pm 0.2$ mag (3.2 ± 0.3 kpc, 3 stars) for Danks 1, Danks 2 and DBS 132, respectively. The error is calculated from a standard deviation of the mean value. Thus we support Davies et al. (2012)'s conclusion that Danks 1 and Danks 2 (and, now, also DBS 132) have the same distance to within the uncertainties. Those distances also corroborate even earlier values obtained by Bica et al. (2004). As for RCW 79, we adopt the spectral classification of the stars observed by Martins et al. (2010) to determine the distance, and get $(m - M)_0 = 13.4 \pm 0.4$ mag (4.8 ± 0.8 kpc).

3.5. Ages

The age can be estimated by fitting the observed CMD with solar-metallicity Geneva isochrones (Lejeune & Schaerer 2001) with combination with PMS isochrones (Seiss et al. 2000). Starting with the isochrones set to the previously determined distance modulus and reddening, we apply shifts in magnitude and color until the fitting statistics reach a minimum value (i.e. difference in magnitude and color of the stars from the isochrone should be minimal) for both the main sequence and PMS isochrones. We get an age of 1-5 Myr for Danks 1, 4-7 Myr for Danks 2, 1-3 Myr for DBS 132 and 2-4 Myr for RCW 79. Figure 9 shows the isochrone fits superimposed on the decontaminated CMDs for all clusters. As can be seen in the figure, however, for such young star clusters the main sequence isochrones are almost vertical lines in near-infrared and it is hard to determine the precise age even using the PMS isochrone set. For this reason and following Liermann et al. (2012) we constructed the HR diagrams for the most luminous stars in Danks 1, Danks 2 and RCW 79. They are plotted in Figure 10. The effective temperatures for the early-type OB type stars were determined from the spectral types of the stars according to the spectral-type-temperature calibration of Martins et al. (2005) and the bolometric corrections are calculated using the equation 2 of Liermann et al. (2012) and their correction to the BC_K . The bolometric corrections for WR stars are taken from Martins et al. (2008). Absolute stellar magnitudes were derived from the K_s magnitudes given in Table 2 with the individual extinction and distance derived from their spectral types. Then we compare the distribution of the stars with the latest isochrones and stellar tracks (with rotation) taken from Ekström et al. (2012). The temperature and luminosities of RCW 79 are taken directly from Martins et al. (2010), here we repeated their Fig. 7 just to be in the same isochrones and stellar tracks system. As can be seen the most of the stars are concentrated around 3, 5 and 4 Myr isochrones for Danks 1, Danks 2 and RCW 79 respectively. Comparing with Davies et al. (2012) age determination, we derived slightly older ages for Danks 1 and Danks 2, but taking in to

Table 3. Proper motion and RV components

| Name | N stars | Mean ($\mu_\alpha \cos \delta$) mas yr ⁻¹ | $\sigma_{\mu_\alpha \cos \delta}$ mas yr ⁻¹ | Mean (μ_δ) mas yr ⁻¹ | σ_{μ_δ} mas yr ⁻¹ | Mean (RV) km s ⁻¹ | σ_{RV} km s ⁻¹ |
|--------|------------|---|---|---|---|---------------------------------|-------------------------------------|
| Field | 194 | -21±1 | 11±1 | -7±1 | 10±1 | — | — |
| Danks1 | 9 | -28±2 | 12±3 | -16±4 | 19±4 | -42±1 | 5.0±0.5 |
| Danks2 | 18 | -23±1 | 6±1 | -11±1 | 7±1 | -44±1 | 8.0±1.0 |
| DB132 | 5 | — | — | — | — | -55±5 | 2.0±1.0 |

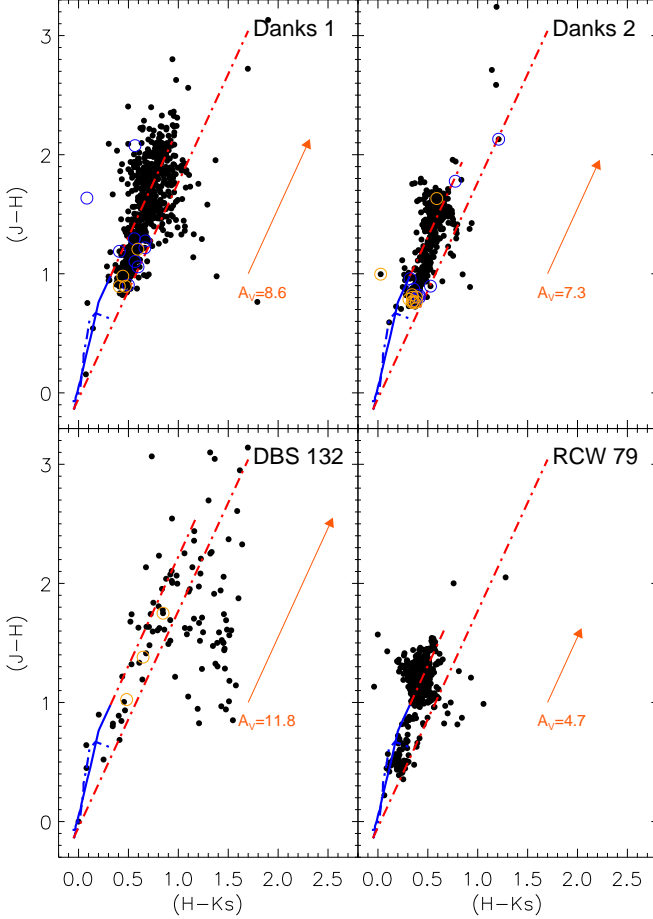


Fig. 8. $(J-H)$ vs. $(H-K_s)$ color-color diagram. The continuous lines represents the sequence of the zero-reddening stars of luminosity class I and class V (Koornneef 1983). The reddening vector is overplotted and the dotted lines are parallel to the standard reddening vector. O and B stars are marked with blue and orange circles, respectively.

account large uncertainties of age determinations, we consider our results in good agreement. Martins et al (2010) also derived younger age for RCW 79 (2.3 ± 0.5 Myr), but again, is consistent with our determination within the errors.

3.6. Initial mass function and cluster masses

By looking at the clusters' CMDs it was often obvious which stars were not genuine cluster members or were not MS objects. Some of these spurious objects are by-products of our decontamination method (see section 2.1.2). There were also some Wolf-Rayet stars that needed to be removed. The LF was converted to

the Initial Mass Function (IMF) using the Geneva isochrones assuming solar metallicity for ages 3, 5, 4 and 2 Myrs for Danks 1, Danks 2, RCW 79 and DBS 132 respectively. For each cluster we established the MS turn-on point and assumed everything fainter than this to be PMS. This point was found to be at $K_s \sim 14$ for Danks 1, Danks 2 and DB 132, and $K_s \sim 13$ for RCW79.

Our calculated slopes of $\Gamma = -1.43 \pm 0.17$ for Danks 1 and $\Gamma = -1.23 \pm 0.22$ for Danks 2, consistent with the Salpeter slope ($\Gamma = -1.35$) to within 1σ as well as with Davies et al. (2012) results. These slopes were used to extrapolate the masses of the observed MS stars to provide a total mass for the cluster. For extrapolation of masses below $<0.5 M_\odot$ we used the Kroupa value of $\Gamma = -0.3$. This gave a total mass of $7900^{+1400}_{-1050} M_\odot$ for Danks 1 and $2900^{+850}_{-550} M_\odot$ for Danks 2. The results are in very good agreement with those found in Davies et al. (2012), i.e. $8000 \pm 1500 M_\odot$ and $3000 \pm 800 M_\odot$ for Danks 1 and Danks 2.

RCW 79 has a slope of $\Gamma = -1.05 \pm 0.28$, with a mass of $3000^{+950}_{-450} M_\odot$. DB 132 did not contain enough stars to reliably estimate a slope, nor completeness for each magnitude band. However, using the same methodology as demonstrated above, we suggest a minimum mass of $\sim 400 M_\odot$.

It should be noted that despite the fact we refer to the true IMF of these clusters that even due to the young age of the clusters, the stellar mass function cannot be considered to be the IMF. Dynamical evolution of the cluster will result from the loss of stars through equipartition of energy, resulting in a higher average star-mass and an increase in binarity proportion. This will affect the slope of the stellar mass function (causing it to flatten). This is sensitive to both mass and cluster lifetime (in particular for those with $<10^4 M_\odot$ and life-times of a few 100 Myr; Kroupa et al. 2011) so this must be considered for these clusters.

Table 4. Physical parameters of the clusters

| Cluster | Slope | Mass (PMS) M_\odot | Mass (MS) M_\odot | Total Mass M_\odot |
|---------|------------------|-------------------------|------------------------|-------------------------|
| Danks 1 | -1.43 ± 0.17 | 900^{+50}_{-30} | 7000^{+1450}_{-1000} | 7900^{+1400}_{-1050} |
| Danks 2 | -1.23 ± 0.22 | 600^{+50}_{-50} | 2300^{+800}_{-500} | 2900^{+850}_{-550} |
| RCW 79 | -1.05 ± 0.28 | 500^{+200}_{-100} | 2500^{+750}_{-300} | 3000^{+950}_{-450} |
| DB 132 | -0.97 ± 0.39 | >60 | >265 | >345 |

4. Search for variable stars

The VVV survey provides many epochs of observations in the K_s -band. So far, now that the second year of the survey is completed, a small fraction of the total number of expected epochs have been obtained in the Galactic disk. This could be enough to look for variable candidates and perhaps some periodicities. An observation log of the K_s observations of the two VVV fields which contain the clusters studied in this paper is presented in

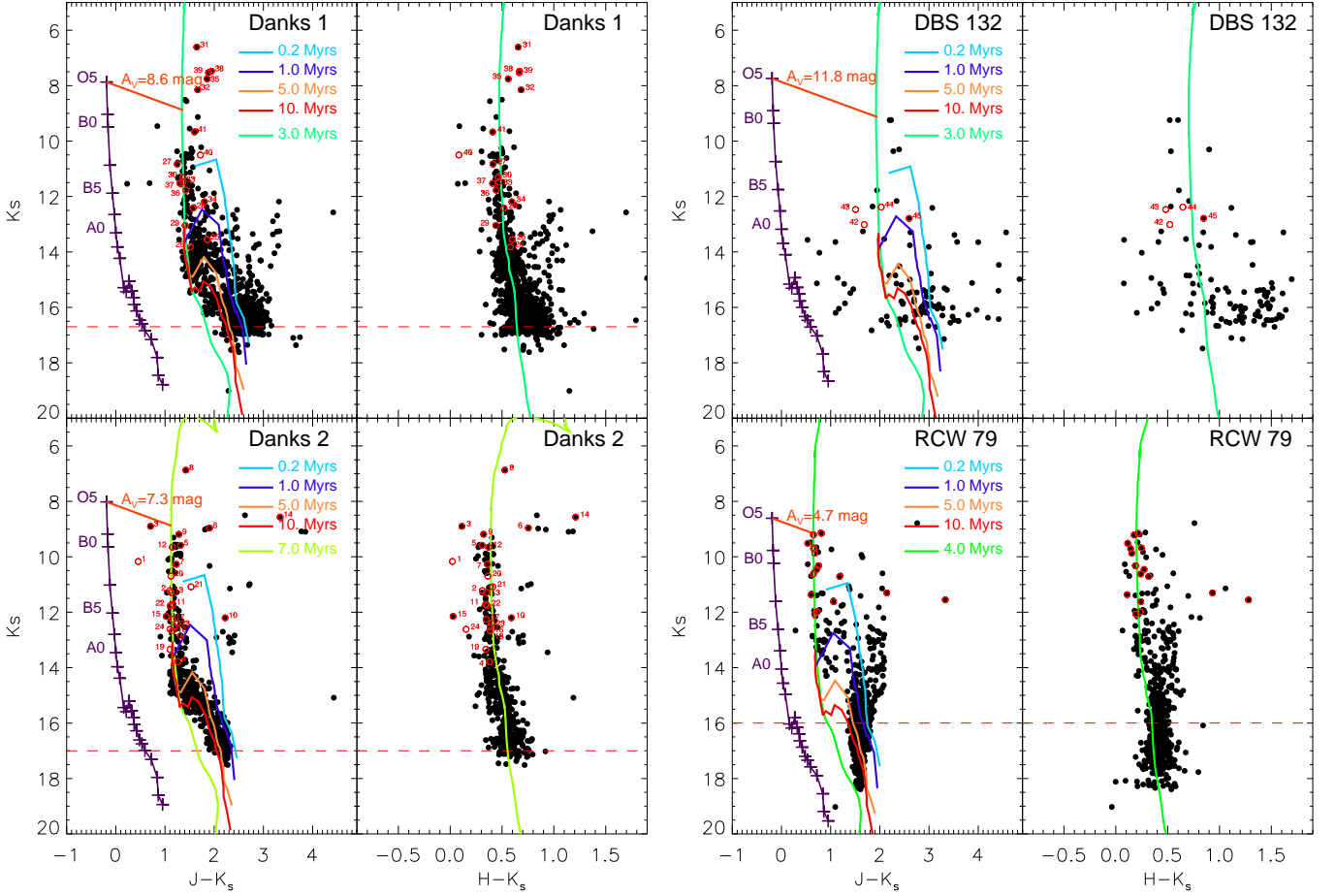


Fig. 9. The color-magnitude diagrams for the four studied clusters. The Schmidt-Kaler (1982) sequence is shown in the $(J - K_s)$ vs. K_s diagram. Red circles mark the stars for which spectra have been observed, and the number attached to them refers to the name of the star listed in Table 2. The red dashed lines represent 50% completeness limit. The green line is the main-sequence model (the exact color changes with the age used), whereas the others (light blue, dark blue, orange and read) are PMS models. See text for more details.

Table 1. Among the VVV-SkZpipeline’s outputs is a table of calibrated magnitudes of individual K_s -band frames. Unfortunately, not all observations were obtained in the weather conditions required for the VVV survey and about half of them had to be rejected. To verify our method for calibrating the K_s -band photometry in each individual frame, we verified that all frames share the same magnitude zero-point value by subtracting the magnitude of all observed stars with $12.5 \text{ mag} < K_s < 14.5 \text{ mag}$. For all frames, we get offsets close to 0, with an error comparable to the photometric accuracy. Figure 11 shows the standard deviation, σ_{K_s} , as a function of the mean value, K_s , of the extracted light curves. A grayscale plot is used for better visibility. A theoretical relation between K_s and the photometric accuracy can be obtained starting with the definition of magnitude:

$$K_s = -2.5 \log FI + R + m_0, \quad (3)$$

where F is the mean value of the flat-field, R , the mean value of the readout, m_0 , the magnitude zero-point and I is the integrated observed total flux of a given star. Using the propagation of error formula we obtain:

$$\sigma_{K_s} = \frac{2.5 \log e}{I} \sqrt{(\sigma_F I)^2 + I + \sigma_R^2}, \quad (4)$$

where σ_F is the error on the flat-field (here, assumed to be 1%) and $\sigma_R = \left[\sqrt{\pi} (\text{size of the seeing}) \times (\text{readnoise per pixel}) \right]$ is the

error on the readout. The only value that needs to be fitted to the data is m_0 , and values of 23.8 mag and 23.5 mag were found for d084 and d086, respectively. This function is overplotted on the data in Figure 11 using a solid green line. Due to saturation effects, the observed values of σ_{K_s} deviate from Equation (4) when K_s is brighter than $\sim 12.5 \text{ mag}$. Hence, for these magnitudes, we rather use a logarithmic function derived from fitting a slope to the $\log \sigma_{K_s}$ relation. Using this relation, one could determine a first list of candidate variables, setting a threshold at $5 \times \sigma_{K_s}$. Stars meeting this criteria are marked with filled red circles in Figure 11. However, in addition to the intrinsic variability of stars, σ_{K_s} contains systematic uncertainties that vary, depending on the position of the star on the detector (due to varying read noise and/or flat-field properties and/or presence of varying local background due to a nearby bright/saturated star). Hence, we adopt the approach described in Dékány et al. (2011). During each acquisition of VVV data for fields d084 and d086, we systematically get for each epoch two frames within a few minutes. This allows us to get the internal scatter of the time-series, σ_i , defined as:

$$\sigma_i = \sum_{j=1}^{N-1} (m_j - m_{j+1})^2 / 2M, \quad (5)$$

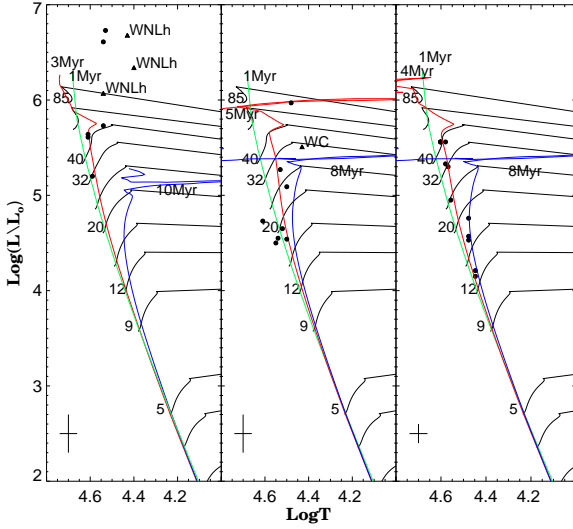


Fig. 10. Hertzsprung-Russell diagrams for the Danks1, Danks2 and RCW79. Circles represent the early-type O stars, triangles the WR stars. The isochrones and stellar evolutionary tracks are from Ekström et al. (2012).

where m_j is the magnitude of the j -th detection. The sum is evaluated for M pairs of detections, each obtained within less than 5 minutes of each other. Candidate variable stars with $\sigma_{K_s}/\sigma_i \geq 2.5$ are shown as blue dots in Figure 11.

Unfortunately, due to bad weather, light curves rarely have more than 15 data points of an appropriate accuracy. Periodograms are very noisy and do not show any clear signal. On the other hand, some long term and/or high amplitude variations can be identified. We add to the Online Material a list of variable candidates contained in the four clusters, along with a brief description of their variations. Also, for both VVV regions studied, i.e. d084 and d086, we find a fraction of 1.5% and 2% of variable sources, respectively, which is in a agreement with the results of Dékány et al. (2011) and Pietrukowicz et al. (2011).

5. Discussion

5.1. The G305 star forming complex

This study provides additional information about the G305 star forming complex. In addition to the diffuse population of massive stars mentioned in Davies et al. (2012, see also Shara et al. 2009 and Mauerhan et al. 2011) our spectral observations reveal 12 early B stars with distances that are comparable with Danks 1 and Danks 2 and thus although not cluster members they are definitely members of the G305 star forming complex. At this stage it is hard to confirm or reject their runaway status, because we cannot yet measure the proper motions using VVV data. Alternatively, they can be part of a larger association of young stars surrounding Danks 1 and 2 formed within the same molecular cloud. Taking advantage of the VVV wide field of view, we examined the stellar content of the regions outlined by Hindson et al. (2010). In addition to the already catalogued clusters, namely: Danks 1, Danks 2, DBS 83, DBS 84, DBS 130, DBS 131 (IR cluster G305.24+0.204, Clark et al. 2004, Leistra et al. 2005, Longmore et al. 2007), DBS 132, DBS 133, DBS 134, cluster G305.363+0.179 (Clark et al. 2004) we have found three new young star clusters and/or stellar groups: VVV CL023, VVV CL022, VVV CL021 (Borissova et al. 2011), and a new star forming region SFR1. The preliminary

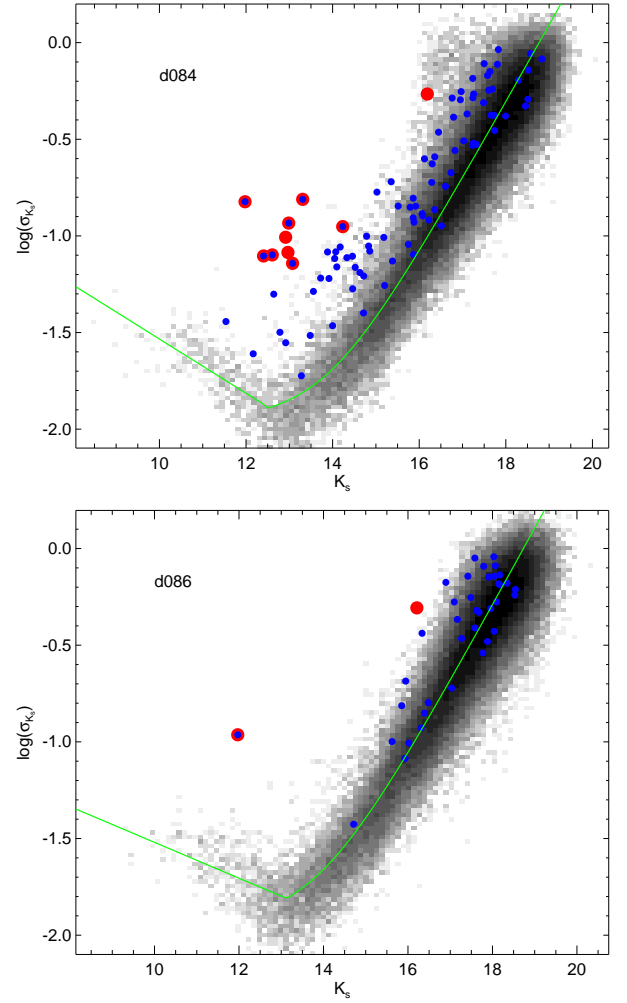


Fig. 11. Standard deviation (σ_{K_s}) of the K_s -band light-curve extracted from the VVV fields d084 and d086. The fit of a theoretical relation between the K_s and the photometric accuracy is plotted in solid, green line. The variable candidates among the stars in the radius of the four studied clusters are shown. Big, red circles are stars having a variability amplitude higher than $5\sigma_{K_s}$, while small, blue circles are stars with $\sigma_{K_s}/\sigma_i \geq 2.5$, where σ_i is the internal scatter of the time-series.

VVV CMD of G305.24+0.204 (DBS 131) is shown in Figure 12, where in addition to a well defined MS highlighted previously by Leistra et al. (2005) and Longmore et al. (2007) the PMS population is readily apparent in the VVV data. The adopted parameters of the plot are $m - M = 12.85$ mag (3.72 kpc), $E(J - K) = 2.25$ mag, age 3–5 Myr. DBS 131, as well as all other clusters from the G305 complex listed here are very young (less than 5 Myr) and less massive than Danks 1 and Danks 2. A more detailed analysis of these objects will be presented in the next paper in our series (Borissova et al., in preparation).

5.2. Milky Way's structure

The clusters' context within the Milky Way's structure is now assessed. The depth of the VVV photometry permits the mapping of crowded low latitude Galactic fields (Minniti et al. 2011). The youth of the stellar constituents inferred from the spectral types (Table 2) implies that Danks 1 and Danks 2 are viable tracers of the Galaxy's spiral structure. Georgelin et al. (1988) first

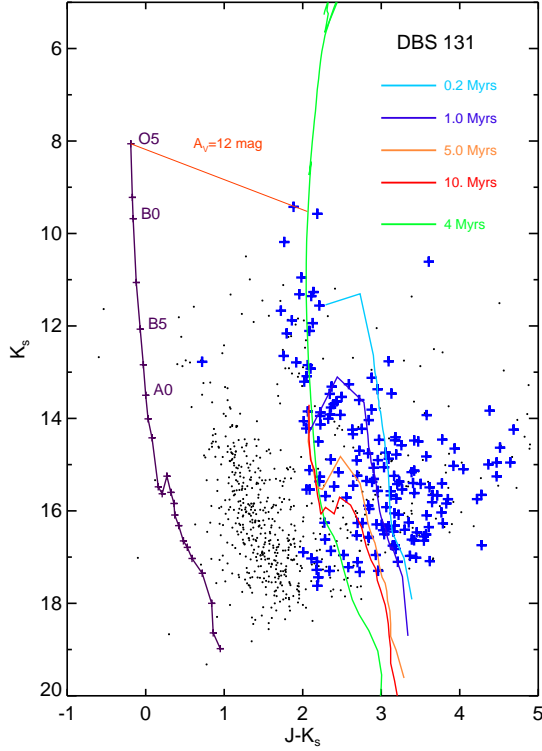


Fig. 12. $(J - K_s)$ vs. K_s diagram for DBS 131, presented as in Figure 9. Dark dots are field stars and blue crosses are cluster stars.

mentioned that the G305 region should be within the Scutum-Crux arm of the Galaxy. Later, Baume et al. 2009 noted that Danks 1 and Danks 2 may belong to the Carina spiral arm. That conclusion is tied to their distance, which is significantly nearer ($> 50\%$) than that found here. Their optical distance is acutely sensitive to variations in R_V , particularly since the total extinction in the optical $A_V = R_V \times E(B - V)$ is sizable, and because it is not constrained by any spectroscopic observation. The present results support the larger distance cited by Davies et al. (2012). The positions of Danks 1 and Danks 2 are plotted in Figure 13 on a hybrid map of the Galaxy’s spiral structure as delineated by long-period classical Cepheids and young (< 10 Myr) open clusters. Long-period Cepheids are more massive younger stars than their shorter period counterparts since the variables follow a period-luminosity relation. Cepheid variables and young open clusters define an analogous (local) spiral pattern (e.g. Majaess et al. 2009). Danks 1 and Danks 2 lie beyond the Sagittarius-Carina spiral arm and occupy the Centaurus arm, along with numerous young Cepheids and clusters (e.g., TW Nor, VW Cen, and VVV CL070). VVV CL070 was discovered in the comprehensive survey by Borissova et al. (2011), who discovered 96 new clusters in the region sampled by the VVV survey.

6. Summary

In this paper we are reporting the study of three young, known massive star clusters using data from the VVV survey and complementary low-resolution near-IR spectroscopy. The two of the clusters, namely Danks 1 and Danks 2 were investigated by Davies et al. (2012), while RCW 79 has excellent spectroscopic observations of brightest members (Martins et al. 2010). We choose these clusters to test and describe our methodology,

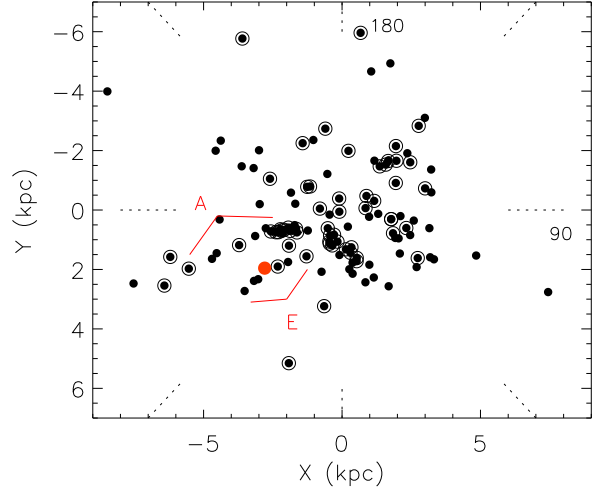


Fig. 13. Map of local spiral structure as delineated by long period classical Cepheids (dots) and young clusters (circled dots) (see also Majaess et al. 2009). The Carina (A) and Centaurus (E) spiral arms are indicated on the diagram. Danks 1 and Danks 2 (red dot) reside in the Centaurus spiral arm.

which we will employ to study hundreds of open clusters observed by the VVV survey. The new analysis of Danks 1 and Danks 2 can be compared with Davies et al. (2012)’s work. First, we obtain comparable values of reddening. However, our results are based on many more spectra and use both VVV JHK_s CMDs and CCDs. Our results account for differential reddening and the reddening laws were established for the line of sight, thus mitigating uncertainties from propagating into the distance determination. Second, we also obtain similar distances. But, while their analysis was limited by the uncertainty on the luminosity class assignment, since they mostly observed bright stars that are near the turnoff, ours is less influenced by this problem, since we have access to spectra of many B dwarf stars. The cluster membership is derived using both radial velocity and proper motion analysis. The agreement with Davies et al. (2012)’s results also calls into question the much smaller distances determined by Baume et al. (2009). Third, we derive comparable masses. We found that Danks 1 and Danks 2 have 3 and 5 Myr respectively. Those values are slightly older comparing with the ages reported by Davies et al. (2012), but still agree within the errors. Taking advantage of large field of view of VVV we reported a large population of pre-main sequence stars. Interestingly enough Danks 2 contains the highest fraction (16% of the total mass) in PMS population, followed by RCW 79 (15%) and Danks 1 (only 4%). Based on radial velocity analysis, we found that Danks 1 and Danks 2 have the same mean radial velocity, which indicates that they are indeed binary clusters. A list of candidate variable stars is proposed, which will be confirm with collecting more VVV images, during the continuation of the survey. We also report our results for DBS 132 and DBS 131, open clusters situated close to the two Danks’ clusters. Both clusters are very young (1-3 Myr), still embedded in dust and gas, and least massive than Danks’ clusters. In addition to the diffuse population of massive WR stars, our spectral observations reveal 12 early B stars with distances that are comparable with Danks 1 and Danks 2 and thus although not cluster members they are definitely members of the G305 star forming complex. The G305 complex most probably lies beyond the Sagittarius-Carina spiral

arm and occupy the Centaurus arm. Finally, we present the first deep infrared color-magnitude diagram of RCW79, revealing a large pre-main sequence population. We calculated the mass of the cluster of approx. $3000 M_{\odot}$.

Acknowledgements. This project is supported by the Chilean Ministry for the Economy, Development, and Tourism's Programa Iniciativa Científica Milenio through grant P07-021-F, awarded to The Milky Way Millennium Nucleus. ANC gratefully acknowledges support from the Chilean Centro de Astrofísica FONDAP No. 15010003 and the Chilean Centro de Excelencia en Astrofísica y Tecnologías Afines (CATA) and Comité Mixto ESO-GOBIERNO DE CHILE. JB is supported by FONDECYT No. 1120601 and by the Ministry for the Economy, Development, and Tourism's Programa Iniciativa Científica Milenio through grant P07-021-F, awarded to The Milky Way Millennium Nucleus. JRAC is also supported by FONDECYT Regular #1080086. RK is supported by Centro de Astrofísica de Valparaíso and Proyecto DIUV23/2009. DG also acknowledges FONDAP and CATA funds. DM is supported by FONDECYT Regular #1090213, by the FONDAP Center for Astrophysics #15010003, by the BASAL CATA Center for Astrophysics and Associated Technologies PFB-06, and by the MILENIO Milky Way Millennium Nucleus from the Ministry of Economy's ICM grant P07-021-F. RdG acknowledges partial research support through grant 11073001 from the National Natural Science Foundation of China. MSNK is supported by a Ciência 2007 contract, funded by FCT/MCTES (Portugal) and POPH/FSE (EC). The data used in this paper have been obtained with NTT/SoFi at the ESO La Silla Observatory, and with Clay/MMIRS at Las Campanas Observatory. This research has made use of the SIMBAD database, operated at CDS, Strasbourg, France. We gratefully acknowledge use of data from the ESO Public Survey programme ID 179.B-2002 taken with the VISTA telescope, and data products from the Cambridge Astronomical Survey Unit.

References

- Baume, G., Carraro, G., & Momany, Y. 2009, *MNRAS*, 398, 221
- Bessell, M.S., Castelli, F., & Plez, B. 1998, *A&A*, 333, 231
- Bica, E., Ortolani, S., Momany, Y., Dutra, C. M. & Barbuy, B. 2004, *MNRAS*, 352, 226
- Bik, A., Kaper, L., Hanson, M. M. & Smits, M. 2005, *A&A*, 440, 121
- Bonatto C. & Bica E. 2010, *A&A*, 516, 81
- Bonatto, C., & Bica, E. 2011, *MNRAS*, 415, 313
- Borissova, J., Bonatto, C., Kurtev, R. et al. 2011, *A&A*, 532A, 131
- Borissova, J., Georgiev, L., Hanson, M. M., Clarke, J. R. A., Kurtev, R., Ivanov, V. D., Hillier, D. J., & Penaloza, F. 2012, *A&A*, submitted
- Catelan, M., Minniti, D., Lucas, P. W. et al. 2011, in *Carnegie Observatories Astrophysics Series*, Vol. 5, RR Lyrae Stars, Metal-Poor Stars, and the Galaxy, ed. A. McWilliam, 145
- Clark, J. S. & Porter, J. M. 2004, *A&A*, 427, 839
- Cardelli, J. A., Clayton, G. C., & Mathis 1989, *ApJ*, 345, 245
- Crowther, P., Hadfield, L., Clark, J., S. Negueruela, I. & Vacca, W. 2006, *MNRAS*, 372, 1407
- Danks, A. C., Dennefeld, M., Wamsteker, W., & Shaver, P. A. 1983, *A&A*, 118, 301
- Davies, B., Clark, J. S.; Trombley, C. et al. 2012, *MNRAS*, 419, 1871
- Dekany, I., Catelan, M., Minniti, D. & the VVV Collaboration 2011, *arXiv:1111.0909v2*
- Dias, W. S., Alessi, B. S., Moitinho, A., & Lépine, J. R. D. 2002, *A&A*, 389, 871
- Dutra C. M., Santiago B. X. & Bica E. 2002, *A&A*, 383, 219
- Elmegreen 2007, *ApJ*, 668, 1064
- Emerson, J. & Sutherland, W. 2010, *The Messenger*, 139, 2
- Ekström, S., Georgy, C., Eggenberger, P., et al. 2012, *A&A*, 537, A146
- Figer, D. F., McLean, I. S. & Najarro, F., 1997, *ApJ*, 486, 420
- Fischera, J., & Dopita, M. A. 2004, *ApJ*, 611, 919
- Gehrels, N., 1986, *ApJ*, 303, 336
- Georgelin, Y. M., Boulesteix, J., Georgelin, Y. P., Le Coarer, E., & Marcelin, M. 1988, *A&A*, 205, 95
- Girardi, L., Williams, B., Gilbert, K., Rosenfield, P., & Dalcanton, J. 2010, *ApJ*, 724, 1030
- Hanson, M. M., Conti, P. S. & Rieke, M. J. 1996, *ApJS*, 107, 281
- Hanson, M. M., Rieke, M. J. & Luhman, K. L. 1998, *AJ*, 116, 1915
- Hanson, M. M., Kudritzki, R.-P., Kenworthy, M. A., Puls, J. & Tokunaga, A. T. 2005, *ApJS*, 161, 154
- Hanson, M. M., Kurtev, R., Borissova, J., Georgiev, L., Ivanov, V. D., Hillier, D. J., Minniti, D. 2010 *A&A*, 516A, 35
- Hillier, D. J., & Miller, D. L. 1998, *ApJ*, 496, 407
- Hindson, L., Thompson, M. A., Urquhart, J. S., Clark, J. S., & Davies, B. 2010, *MNRAS*, 408, 1438
- Irwin, M. J., Lewis, J., Hodgkin, S., et al. 2004, in *Society of Photo-Optical Instrumentation Engineers (SPIE) Conference Series*, ed. P. J. Quinn & A. Bridger, Vol. 5493, 411
- Ivanov V. D., Kurtev, R., & Borissova, J. 2005, *A&A*, 442, 195
- Koornneef, J. 1983, *A&A*, 128, 84
- King, I. R. 1966, *AJ*, 71, 64
- Kroupa, P., Weidner, C., Pflamm-Altenburg, J., Thies, I., Dabringhausen, J., Marks, M., & Maschberger, T. 2011, *arXiv*, arXiv:1112.3340
- Lada & Lada 2003, *ARA&A*, 41, 57
- Lejeune, A., Schaerer 2001, *A&A*, 366, 538
- Leistra, A., Cotera, A. S., Liebert, J., & Burton, M. 2005, *AJ*, 130, 1719
- Liermann, A., Hamann, W.-R. & Oskinova, L. M. 2009, *A&A*, 494, 1137
- Liermann, A., Hamann, W.-R., & Oskinova, L. M. 2012, *A&A*, 540, A14
- Livingston W. & Wallace L. 1991, National Solar Observatory: "An atlas of the solar spectrum in the infrared from 1850 to 9000 cm⁻¹", Technical Report #91-001)
- Longmore, S. N., Maercker, M., Ramstedt, S., & Burton, M. G. 2007, *MNRAS*, 380, 1497
- Longmore, A. J., Kurtev, R., Lucas, P. W., Froebrich, D., de Grijs, R., Ivanov, V. D. V. D., Maccarone, T. J., Borissova, J., Ker, L. M. 2011 *MNRAS*, 416, 465
- Maiolino, Rieke & Rieke 1996, *AJ*, 111, 537
- Majaess, D. J., Turner, D. G., & Lane, D. J. 2009, *MNRAS*, 398, 263
- Majaess, D. J., Turner, D., Moni Bidin, C. et al. 2011, *ApJ*, 741L, 27
- Majaess, D. J., Turner, D., Moni Bidin, C. et al. 2012, *A&A*, 537L, 4
- Martins, F., Schaerer, D., & Hillier, D. J. 2005, *A&A*, 436, 1049
- Martins, L. P. & Coelho, P. 2007, *MNRAS*, 381, 1329
- Martins, F., Hillier, D. J., Paumard, T., et al. 2008, *A&A*, 478, 219
- Martins, F., Pomarès, M., Deharveng, L., Zavagno, A., & Bouret, J.-C. 2010, *A&A*, 510, 32
- Mauerhan, J., Van Dyk, S. & Morris, P. 2011, *AJ*, 142, 40
- Mauro, F., Moni Bidin, C., Chené, A.-N et al. 2012, *PASP*, submitted
- Monnier, J. D., Tuthill, P. G., Danchi, W. C., Murphy, N., Harries, T. J. 2007, *ApJ*, 655, 1033
- Minniti, D., Lucas, P. W., Emerson, J. P., et al. 2010, *New A*, 15, 433
- Minniti, D., Saito, R., Alonso-García, J., Lucas, P. W., & Hempel, M. 2011, *ApJ*, 733L, 43
- Morris, Patrick W., Eenens, P. R. J., Hanson, Margaret M., Conti, Peter S. & Blum, R. D. 1996, *ApJ*, 470, 597
- Moorwood, A., Cuby, J.-G., & Lidman, C. 1998, *The Messenger*, 91, 9
- Negueruela, I., González-Fernández, C., Marco, A., & Clark, J. S. 2011, *A&A*, 528, A59
- Negueruela, I., Marco, A., Israel, G. L., Bernabeu, G., 2007, *A&A*, 471, 485
- Roeser, S., Demleitner, M., & Schilbach, E. 2010, *AJ*, 139, 2440
- Pietrukowicz, P., Minniti, D., Alonso-García, J., & Hempel, M. 2012, *A&A*, 537A, 116
- Portegies Zwart et al. 2010, *ARA&A*, 48, 431
- Price & Bate 2009, *MNRAS*, 398, 33
- Ramírez Alegría, S., Marín-Franch, A., & Herrero, A. 2012, *A&A*, 541A, 75
- Rayner, J. T., Cushing, M. C., & Vacca, W. D. 2009, *ApJS*, 185, 289
- Rieke, G. H. & Lebofsky, M. J. 1985, *ApJ*, 288, 618
- Sana, H., James, G., & Gosset, E. 2011, *MNRAS*, 416, 817
- Saito, R. K., Hempel, M., Minniti, D. et al. 2012, *A&A*, 537A, 107
- Schmidt-Kaler, T., 1982, in *Landolt-Borstein, New Series*, Group VI, vol. 2, ed. K. Schaifers & H.H. Voigt (Berlin: Springer-Verlag), 1
- Schnurr, O., Moffat, A. F. J., St-Louis, N., Morrell, N. I. & Guerrero, M. A. 2008, *MNRAS*, 389, 806
- Shara, M. M., Moffat, A. F. J., Gerke, J. et al. 2009, *AJ*, 138, 402
- Siess L., Dufour E., & Forestini M. 2000, *A&A*, 358, 593
- de Silva, G. M., Gibson, B. K., Lattanzio, J., & Asplund, M. 2009, *A&A*, 500L, 25
- Stetson, P. B. 1994, *PASP*, 106, 250
- Straizys, V., & Lazauskaitė, R. 2008, *Baltic Astronomy*, 17, 253
- Straizys, V., & Lazauskaitė, R. 2009, *Baltic Astronomy*, 18, 19
- Turner, D. G. 1976, *AJ*, 81, 1125
- Turner, D. G. 1989, *AJ*, 98, 2300
- Turner, D. G. 2011, *RMxAA*, 47, 127
- van der Hucht, K. A. 2001, *NewAR*, 45, 135
- Williams, P. M., van der Hucht, K. A., van Wyk, F., Marang, F., Whitelock, P. A., Bouchet, P., Setia Gunawan, D. Y. A. 2012, *MNRAS*, in press
- de Wit, W. J., Testi, L., Palla, F., & Zinnecker, H. 2005, *A&A*, 437, 247
- Yadav R. K. S. & Sagar R. 2001, *MNRAS*, 328, 370
- Zhekov, S. A., Gagn, M., & Skinner, S. L. 2011, *ApJ*, 727L, 17

Table 1. Observation log. Columns include UT date, HJD-2.455e6, airmass, seeing in arcsec, ellipticity and quality grade provided by ESO. Both the d084 and d086 fields are presented.

| VVV field d084 | | | | | | VVV field d086 | | | | | |
|----------------|-------------|-------|--------|------|----|----------------|-------------|-------|--------|------|-----|
| UT Date | HJD-2.455e6 | AM | Sng | Ell. | QG | UT Date | HJD-2.455e6 | AM | Sng | Ell. | QG |
| 29 Mar 2010 | 284.092893 | 1.550 | 0.91'' | 0.05 | A | 23 Apr 2010 | 309.040379 | 1.552 | 0.67'' | 0.08 | A |
| 29 Mar 2010 | 284.093200 | 1.547 | 0.85'' | 0.06 | A | 23 Apr 2010 | 309.040738 | 1.548 | 0.69'' | 0.09 | A |
| 7 Apr 2010 | 293.088925 | 1.462 | 0.89'' | 0.08 | C | 11 May 2010 | 327.158628 | 1.269 | 0.76'' | 0.17 | C |
| 7 Apr 2010 | 293.089231 | 1.459 | 0.94'' | 0.06 | C | 11 May 2010 | 327.158984 | 1.268 | 0.80'' | 0.15 | C |
| 7 Apr 2010 | 293.091056 | 1.454 | 1.12'' | 0.07 | C | 12 May 2010 | 328.150803 | 1.265 | 0.77'' | 0.13 | C |
| 7 Apr 2010 | 293.091364 | 1.451 | 0.92'' | 0.10 | C | 12 May 2010 | 328.151117 | 1.264 | 0.78'' | 0.11 | C |
| 7 Apr 2010 | 293.093232 | 1.446 | 0.95'' | 0.12 | C | 9 Jun 2010 | 356.088306 | 1.277 | 0.92'' | 0.19 | C |
| 7 Apr 2010 | 293.093539 | 1.444 | 0.89'' | 0.10 | C | 9 Jun 2010 | 356.088670 | 1.276 | 0.95'' | 0.25 | C |
| 11 May 2010 | 327.149710 | 1.283 | 0.67'' | 0.12 | C | 16 Jun 2010 | 363.096838 | 1.317 | 0.76'' | 0.20 | C |
| 11 May 2010 | 327.150016 | 1.282 | 0.73'' | 0.14 | C | 16 Jun 2010 | 363.097294 | 1.317 | 0.75'' | 0.15 | C |
| 12 May 2010 | 328.137896 | 1.275 | 0.84'' | 0.06 | C | 21 Jun 2010 | 368.087491 | 1.326 | 0.93'' | 0.08 | A |
| 12 May 2010 | 328.138247 | 1.274 | 1.13'' | 0.17 | C | 21 Jun 2010 | 368.087910 | 1.325 | 1.06'' | 0.03 | A |
| 8 Jun 2010 | 355.964570 | 1.328 | 0.91'' | 0.08 | C | 13 Jul 2010 | 390.036517 | 1.346 | 0.79'' | 0.09 | C |
| 8 Jun 2010 | 355.964937 | 1.326 | 0.93'' | 0.14 | C | 13 Jul 2010 | 390.036977 | 1.346 | 0.80'' | 0.05 | C |
| 16 Jun 2010 | 363.080558 | 1.326 | 0.74'' | 0.16 | C | 15 Aug 2010 | 423.990697 | 1.499 | 0.72'' | 0.11 | B |
| 16 Jun 2010 | 363.080968 | 1.325 | 0.73'' | 0.22 | C | 15 Aug 2010 | 423.991116 | 1.500 | 0.75'' | 0.08 | B |
| 21 Jun 2010 | 368.063868 | 1.320 | 0.92'' | 0.11 | C | 17 Aug 2010 | 425.010078 | 1.607 | 0.69'' | 0.07 | A |
| 21 Jun 2010 | 368.064288 | 1.319 | 0.95'' | 0.12 | C | 17 Aug 2010 | 425.010549 | 1.609 | 0.74'' | 0.08 | A |
| 8 Jul 2010 | 385.063093 | 1.439 | 0.76'' | 0.07 | B | 15 May 2011 | 696.219013 | 1.402 | 0.60'' | 0.13 | A |
| 8 Jul 2010 | 385.063579 | 1.439 | 0.77'' | 0.05 | B | 15 May 2011 | 696.219447 | 1.402 | 0.57'' | 0.11 | A |
| 9 Jul 2010 | 386.054580 | 1.419 | 0.62'' | 0.13 | A | 16 Jul 2011 | 758.067592 | 1.464 | 1.15'' | 0.11 | C |
| 9 Jul 2010 | 386.055029 | 1.420 | 0.57'' | 0.08 | A | 16 Jul 2011 | 758.068015 | 1.465 | 1.22'' | 0.09 | C |
| 10 Jul 2010 | 387.063990 | 1.462 | 0.60'' | 0.12 | A | 30 Jul 2011 | 772.017268 | 1.420 | 0.69'' | 0.05 | A |
| 10 Jul 2010 | 387.064418 | 1.462 | 0.64'' | 0.11 | A | 30 Jul 2011 | 772.017713 | 1.421 | 0.73'' | 0.13 | A |
| 10 Aug 2010 | 418.007474 | 1.588 | 0.79'' | 0.19 | A | 31 Jul 2011 | 773.009639 | 1.404 | 1.37'' | 0.07 | N/A |
| 10 Aug 2010 | 418.007953 | 1.589 | 0.79'' | 0.14 | A | 31 Jul 2011 | 773.010068 | 1.405 | 1.35'' | 0.08 | N/A |
| 14 Jun 2011 | 726.145651 | 1.502 | 0.73'' | 0.07 | A | 2 Aug 2011 | 775.013248 | 1.435 | 2.30'' | 0.19 | C |
| 14 Jun 2011 | 726.146109 | 1.502 | 0.78'' | 0.07 | A | 2 Aug 2011 | 775.013651 | 1.435 | 2.02'' | 0.20 | C |
| 24 Jul 2011 | 766.025934 | 1.460 | 0.74'' | 0.10 | A | 4 Aug 2011 | 777.022491 | 1.491 | 0.77'' | 0.11 | B |
| 24 Jul 2011 | 766.026379 | 1.460 | 0.75'' | 0.06 | A | 4 Aug 2011 | 777.022898 | 1.492 | 0.70'' | 0.10 | B |
| 7 Aug 2011 | 780.991745 | 1.486 | 0.80'' | 0.13 | A | 15 Aug 2011 | 788.017516 | 1.614 | 0.85'' | 0.09 | B |
| 7 Aug 2011 | 780.992151 | 1.487 | 0.88'' | 0.09 | A | 15 Aug 2011 | 788.017933 | 1.616 | 0.76'' | 0.07 | B |
| 16 Aug 2011 | 789.979686 | 1.541 | 0.88'' | 0.14 | A | 17 Aug 2011 | 790.993083 | 1.531 | 1.16'' | 0.07 | N/A |
| 16 Aug 2011 | 789.980120 | 1.542 | 0.96'' | 0.04 | A | 17 Aug 2011 | 790.993548 | 1.532 | 1.19'' | 0.05 | N/A |
| | | | | | | 21 Aug 2011 | 794.993380 | 1.587 | 0.88'' | 0.11 | A |
| | | | | | | 21 Aug 2011 | 794.993802 | 1.588 | 0.90'' | 0.05 | A |
| | | | | | | 22 Aug 2011 | 795.995700 | 1.615 | 1.56'' | 0.05 | C |
| | | | | | | 22 Aug 2011 | 795.996109 | 1.616 | 1.61'' | 0.09 | C |

Table 2. List of variable candidates in Danks 1 and Danks 2. Columns include RA (J2000), DEC (J2000), Mean (K_s) and $\log \sigma_{K_s}$.

| Catalog number | RA (J2000) | DEC (J2000) | Mean(K_s) | $\log \sigma_{K_s}$ | Catalog number | RA (J2000) | DEC (J2000) | Mean(K_s) | $\log \sigma_{K_s}$ |
|----------------|------------|-------------|---------------|---------------------|----------------|------------|-------------|---------------|---------------------|
| D1-0078 | 198.07936 | -62.706541 | 15.86 | -0.80 | D1-3546 | 198.12989 | -62.701732 | 16.08 | -0.89 |
| D1-0093 | 198.07970 | -62.705462 | 15.20 | -1.25 | D1-3548 | 198.13037 | -62.713030 | 14.07 | -1.08 |
| D1-0093 | 198.08006 | -62.705399 | 15.79 | -0.85 | D1-3540 | 198.13098 | -62.697912 | 14.45 | -1.10 |
| D1-0128 | 198.08058 | -62.705065 | 15.86 | -0.90 | D1-3542 | 198.13103 | -62.700520 | 13.72 | -1.21 |
| D1-0119 | 198.08075 | -62.705865 | 16.28 | -0.72 | D1-3550 | 198.13485 | -62.690548 | 18.83 | -0.08 |
| D1-0112 | 198.08141 | -62.707093 | 16.96 | -0.25 | D1-3546 | 198.13841 | -62.701339 | 11.53 | -1.44 |
| D1-0276 | 198.08377 | -62.696737 | 14.32 | -1.11 | D1-3548 | 198.13906 | -62.711442 | 17.82 | -0.03 |
| D1-0353 | 198.08523 | -62.701102 | 16.22 | -0.91 | D1-3544 | 198.13994 | -62.704730 | 14.52 | -1.16 |
| D1-0365 | 198.08536 | -62.693862 | 13.07 | -1.14 | D1-3542 | 198.14063 | -62.700532 | 14.78 | -1.00 |
| D1-0379 | 198.08566 | -62.704213 | 14.23 | -0.95 | D1-3538 | 198.14074 | -62.709018 | 17.69 | -0.24 |
| D1-0520 | 198.08913 | -62.710759 | 18.51 | -0.29 | D1-3538 | 198.14216 | -62.709617 | 16.76 | -0.28 |
| D1-0605 | 198.09067 | -62.704842 | 16.60 | -0.74 | D1-3548 | 198.14252 | -62.710469 | 17.49 | -0.10 |
| D1-0624 | 198.09105 | -62.699257 | 17.31 | -0.52 | D1-3538 | 198.14332 | -62.709620 | 15.35 | -0.71 |
| D1-0629 | 198.09112 | -62.703998 | 13.27 | -1.72 | D1-3538 | 198.14337 | -62.708983 | 16.79 | -0.38 |
| D1-0719 | 198.09152 | -62.707777 | 16.73 | -0.67 | D1-3544 | 198.14476 | -62.705129 | 16.82 | -0.55 |
| D1-0792 | 198.09356 | -62.712184 | 16.35 | -0.59 | D2-0007 | 198.19466 | -62.686308 | 15.91 | -0.84 |
| D1-0823 | 198.09395 | -62.707737 | 11.97 | -0.82 | D2-0045 | 198.19639 | -62.682487 | 17.74 | -0.45 |
| D1-0840 | 198.09415 | -62.692784 | 14.85 | -1.07 | D2-0061 | 198.19709 | -62.684371 | 14.04 | -1.11 |
| D1-0848 | 198.09432 | -62.709843 | 17.63 | -0.14 | D2-0187 | 198.20026 | -62.678689 | 13.91 | -1.22 |
| D1-0871 | 198.09473 | -62.702318 | 12.60 | -1.09 | D2-0266 | 198.20216 | -62.675668 | 17.65 | -0.37 |
| D1-1124 | 198.09827 | -62.697101 | 17.24 | -0.51 | D2-0342 | 198.20354 | -62.679100 | 18.57 | -0.05 |
| D1-1125 | 198.09835 | -62.703466 | 14.83 | -1.05 | D2-0383 | 198.20495 | -62.670688 | 17.25 | -0.26 |
| D1-1295 | 198.10051 | -62.703707 | 14.17 | -1.05 | D2-0415 | 198.20523 | -62.672838 | 16.06 | -0.88 |
| D1-1328 | 198.10091 | -62.716417 | 16.51 | -0.94 | D2-0658 | 198.20920 | -62.672609 | 17.60 | -0.24 |
| D1-1506 | 198.10326 | -62.696218 | 12.64 | -1.30 | D2-0992 | 198.21392 | -62.666613 | 12.98 | -0.93 |
| D1-1808 | 198.10722 | -62.700764 | 13.88 | -1.08 | D2-1063 | 198.21452 | -62.683190 | 17.99 | -0.38 |
| D1-1941 | 198.10898 | -62.700922 | 14.09 | -1.16 | D2-1519 | 198.22076 | -62.677181 | 17.48 | -0.31 |
| D1-2062 | 198.11031 | -62.714601 | 17.02 | -0.50 | D2-1597 | 198.22225 | -62.689244 | 14.71 | -1.20 |
| D1-2350 | 198.11371 | -62.696060 | 12.40 | -1.10 | D2-1862 | 198.22601 | -62.682288 | 13.30 | -0.81 |
| D1-2413 | 198.11389 | -62.697167 | 17.80 | -0.11 | D2-2029 | 198.22850 | -62.679058 | 14.63 | -1.18 |
| D1-2379 | 198.11411 | -62.717062 | 15.75 | -1.04 | D2-2182 | 198.23048 | -62.682038 | 15.86 | -1.09 |
| D1-2397 | 198.11427 | -62.687730 | 16.35 | -0.86 | D2-2223 | 198.23107 | -62.674319 | 13.55 | -1.28 |
| D1-2408 | 198.11439 | -62.688650 | 12.16 | -1.60 | D2-2299 | 198.23172 | -62.677520 | 17.72 | -0.37 |
| D1-2468 | 198.11514 | -62.712483 | 15.87 | -0.92 | D2-2289 | 198.23204 | -62.694124 | 15.18 | -1.00 |
| D1-2763 | 198.11776 | -62.708380 | 18.45 | -0.32 | D2-2497 | 198.23481 | -62.677910 | 15.51 | -0.84 |
| D1-2801 | 198.11893 | -62.708093 | 13.48 | -1.51 | D2-2528 | 198.23522 | -62.670558 | 17.24 | -0.28 |
| D1-2879 | 198.11967 | -62.699463 | 14.46 | -1.27 | D2-2548 | 198.23541 | -62.671228 | 16.95 | -0.29 |
| D1-2974 | 198.12079 | -62.692725 | 15.02 | -0.77 | D2-2579 | 198.23612 | -62.694739 | 17.22 | -0.53 |
| D1-2974 | 198.12110 | -62.692668 | 15.38 | -1.13 | D2-2599 | 198.23641 | -62.683018 | 14.71 | -1.39 |
| D1-3016 | 198.12155 | -62.707313 | 18.52 | -0.14 | D2-2603 | 198.23733 | -62.690218 | 12.91 | -1.55 |
| D1-3135 | 198.12340 | -62.692690 | 17.57 | -0.17 | D2-2783 | 198.23950 | -62.675108 | 12.78 | -1.49 |
| D1-3361 | 198.12551 | -62.701561 | 17.10 | -0.36 | D2-2824 | 198.24012 | -62.667779 | 16.29 | -0.62 |
| D1-3465 | 198.12752 | -62.697527 | 13.99 | -1.46 | D2-3128 | 198.24442 | -62.694468 | 18.28 | -0.19 |
| D1-3491 | 198.12779 | -62.692769 | 16.12 | -0.60 | D2-3203 | 198.25360 | -62.692373 | 16.44 | -0.46 |
| D1-3554 | 198.12955 | -62.702017 | 17.23 | -0.18 | | | | | |

Table 3. List of variable candidates in RCW 79. Columns include RA (J2000), DEC (J2000), Mean (K_s) and $\log \sigma_{K_s}$.

| Catalog number | RA (J2000) | DEC (J2000) | Mean(K_s) | $\log \sigma_{K_s}$ | Catalog number | RA (J2000) | DEC (J2000) | Mean(K_s) | $\log \sigma_{K_s}$ |
|-------------------|------------|-------------|---------------|---------------------|-------------------|------------|-------------|---------------|---------------------|
| RCW79-0029 | 204.94346 | -61.753372 | 14.71 | -1.42 | RCW79-0445 | 204.98517 | -61.742081 | 18.54 | -0.21 |
| RCW79-0040 | 204.94577 | -61.759210 | 18.17 | -0.13 | RCW79-0477 | 204.98628 | -61.750475 | 15.93 | -1.08 |
| RCW79-0002 | 204.94651 | -61.744302 | 18.04 | -0.42 | RCW79-0520 | 204.98716 | -61.744896 | 17.09 | -0.27 |
| RCW79-0002 | 204.95280 | -61.738925 | 17.48 | -0.25 | RCW79-0548 | 204.98786 | -61.746405 | 17.16 | -0.36 |
| RCW79-0029 | 204.95483 | -61.745262 | 17.68 | -0.32 | RCW79-0634 | 204.98923 | -61.744089 | 16.33 | -0.43 |
| RCW79-0002 | 204.95519 | -61.737823 | 17.77 | -0.53 | RCW79-0641 | 204.98962 | -61.750225 | 15.85 | -0.81 |
| RCW79-0029 | 204.96003 | -61.746189 | 17.58 | -0.04 | RCW79-0669 | 204.99144 | -61.750221 | 17.58 | -0.41 |
| RCW79-0029 | 204.96382 | -61.742056 | 15.94 | -0.68 | RCW79-0748 | 204.99336 | -61.736630 | 18.04 | -0.14 |
| RCW79-0150 | 204.96390 | -61.755874 | 17.87 | -0.48 | RCW79-0847 | 204.99354 | -61.748245 | 17.95 | -0.31 |
| RCW79-0002 | 204.97027 | -61.734321 | 16.02 | -1.00 | RCW79-0886 | 204.99462 | -61.736643 | 18.34 | -0.17 |
| RCW79-0131 | 204.97211 | -61.747668 | 18.14 | -0.18 | RCW79-1028 | 204.99670 | -61.752871 | 16.31 | -0.92 |
| RCW79-0150 | 204.97213 | -61.754339 | 17.03 | -0.72 | RCW79-0982 | 204.99693 | -61.741871 | 16.89 | -0.17 |
| RCW79-0150 | 204.97408 | -61.754537 | 17.26 | -0.46 | RCW79-1019 | 204.99724 | -61.756554 | 11.96 | -0.96 |
| RCW79-0071 | 204.97458 | -61.741244 | 18.09 | -0.27 | RCW79-0991 | 204.99758 | -61.740530 | 15.62 | -0.99 |
| RCW79-0176 | 204.97811 | -61.742926 | 17.79 | -0.09 | RCW79-1088 | 204.99809 | -61.741124 | 18.03 | -0.04 |
| RCW79-0235 | 204.97847 | -61.750456 | 18.17 | -0.18 | RCW79-1056 | 204.99852 | -61.747515 | 17.90 | -0.14 |
| RCW79-0330 | 204.98300 | -61.737352 | 16.47 | -0.79 | RCW79-1207 | 205.00134 | -61.750141 | 17.62 | -0.31 |
| RCW79-0394 | 204.98390 | -61.736090 | 16.39 | -0.85 | RCW79-1399 | 205.00368 | -61.743272 | 17.41 | -0.14 |